

Air Force Institute of Technology

AFIT Scholar

Theses and Dissertations

Student Graduate Works

3-15-2006

Backward Amplification and Beam Cleanup of a Raman Fiber Laser Oscillator using a Multi-Mode Graded Index Fiber Amplifier

Jesse D. S. Morgan III

Follow this and additional works at: <https://scholar.afit.edu/etd>



Part of the [Plasma and Beam Physics Commons](#)

Recommended Citation

Morgan, Jesse D. S. III, "Backward Amplification and Beam Cleanup of a Raman Fiber Laser Oscillator using a Multi-Mode Graded Index Fiber Amplifier" (2006). *Theses and Dissertations*. 3357.
<https://scholar.afit.edu/etd/3357>

This Thesis is brought to you for free and open access by the Student Graduate Works at AFIT Scholar. It has been accepted for inclusion in Theses and Dissertations by an authorized administrator of AFIT Scholar. For more information, please contact AFIT.ENWL.Repository@us.af.mil.



**BACKWARD AMPLIFICATION AND BEAM CLEANUP OF A RAMAN FIBER
LASER OSCILLATOR USING A MULTI-MODE GRADED INDEX FIBER
AMPLIFIER**

THESIS

Jesse D. S. Morgan, III, Captain, USAF

AFIT/GAP/ENP/06-11

DEPARTMENT OF THE AIR FORCE
AIR UNIVERSITY

AIR FORCE INSTITUTE OF TECHNOLOGY

Wright-Patterson Air Force Base, Ohio

APPROVED FOR PUBLIC RELEASE; DISTRIBUTION UNLIMITED

The views expressed in this thesis are those of the author and do not reflect the official policy or position of the United States Air Force, Department of Defense, or the United States Government.

AFIT/GAP/ENP/06-11

**BACKWARD AMPLIFICATION AND BEAM CLEANUP OF A RAMAN FIBER
LASER OSCILLATOR USING A MULTI-MODE GRADED INDEX FIBER
AMPLIFIER**

THESIS

Presented to the Faculty

Department of Engineering Physics

Graduate School of Engineering and Management

Air Force Institute of Technology

Air University

Air Education and Training Command

In Partial Fulfillment of the Requirements for the

Degree of Master of Science (Applied Physics)

Jesse D. S. Morgan, III, BS

Captain, USAF

March 2006

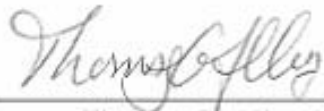
APPROVED FOR PUBLIC RELEASE; DISTRIBUTION UNLIMITED

AFIT/GAP/ENP/06-11

**BACKWARD AMPLIFICATION AND BEAM CLEANUP OF A RAMAN FIBER
LASER OSCILLATOR USING A MULTI-MODE GRADED INDEX FIBER
AMPLIFIER**

Jesse D. S. Morgan, III, BS
Captain, USAF

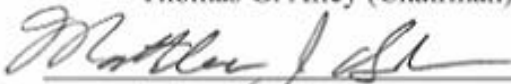
Approved:



Thomas G. Alley (Chairman)

15 Mar '06

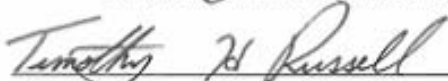
date



Matthew J. Bohn (Member)

15 Mar 06

date



Timothy H. Russell (Member)

15 MAR 06

date

Abstract

This thesis tested a CW fiber-based Raman amplifier implemented in a backward pumped geometry. To create a seed for the amplifier, a CW Nd:YAG laser operating at $1.064\mu\text{m}$ was used to pump a $50\mu\text{m}$ multimode graded index fiber using fiber Bragg gratings to create a Raman Fiber Laser (RFL) Oscillator with a Stokes beam at $1.116\mu\text{m}$. The Stokes beam was then used to seed two lengths, 5.3km and 2.5km, of $50\mu\text{m}$ multimode graded index fiber. The fiber amplifier was pumped by a second CW Nd:YAG laser in the backward geometry.

Spectral data taken for both fibers indicated that the backward geometry avoided the problem of Four Wave Mixing (FWM) present in the forward geometry for amplification. Gain and beam cleanup were observed in both lengths of fiber. An M^2 of 6.7 ± 0.2 was observed in the 5.3km fiber with 5 W of pumping. With 9 W of pump, a gain of 321.3% was observed, but severe attenuation due to the length of fiber prevented overall amplification of the seed with the available pump power. The 2.5km fiber produced an M^2 of 3.9 ± 0.5 with 5 W of pumping. With 10 W of pump, a gain of 241.8% and overall amplification of 153.1% was observed.

Acknowledgments

I would like to express my sincere appreciation to my faculty advisor, Lt Col Tom Alley, for his guidance and encouragement throughout the course of this thesis effort. Also, for his amazing patience and understanding as deadlines came and went. Without his insight and experience, my efforts would not have been as successful.

I'd also like to thank my fellow students for their support; most notably Capt Brent Grime, Capt Nathan Terry, and 1st Lt Brian Flusche. Capt Grime, whose early aid helped me get off the ground and whose thorough knowledge in the lab inspired me to learn more. Capt Terry, who repeatedly took time out of his busy schedule to show me how it was done. Lt Flusche, for helping me to keep all things in perspective. Thank you all, you made more of a difference than any of you will ever know.

I wish to express a special thanks to Dr. Won Roh. The idea for this thesis began with him, and is a part of his legacy as much as anyone. I will never have the level of understanding of this field that he does. Thank you for your many years of dealing with our *ridiculous* fumbling for answers.

I must thank my parents for their generous assistance with last minute editing. But more importantly, I must thank them for their prayers and for raising me in a Godly house with the foundation of values that have left me equipped for a successful life.

Finally, I want to thank my wife and children for supporting me throughout my career and education. Without their patience, I could never have finished. I have no doubt that they will be my greatest legacy in life when everything else is considered.

Jesse D. S. Morgan, III

Table of Contents

	Page
Abstract.....	iv
Acknowledgments.....	v
List of Figures.....	viii
List of Tables	x
I. Introduction	1
Background.....	1
Research Objectives	4
Summary.....	4
Preview	5
II. Literature Review	6
Chapter Overview.....	6
Introduction to Nonlinear Optics.....	6
<i>Stimulated Raman Scattering (SRS)</i>	8
<i>Four Wave Mixing (FWM)</i>	11
Physics of Fibers and Nonlinear Optics	13
Relevant Research	17
Summary.....	18
III. Methodology	19
Chapter Overview.....	19
Raman Fiber Laser Oscillator and Pump Laser Cavity.....	19
Experiment 1: 5.3km Fiber with Polarization Beam Splitters.....	23
Experiment 2: 5.3km Fiber without Polarization Beam Splitters.....	24
Experiment 3: 2.5km Fiber Amplifier	26
Diagnostic Equipment Description.....	27
Summary.....	29
IV. Analysis and Results.....	30
Chapter Overview.....	30
FWM Data.....	30
Spectral Data and Results.....	35

Beam Profiles and Beam Quality	42
Results of Power Measurements	45
Summary.....	48
V. Conclusions and Recommendations	50
Conclusions	50
Future Suggested Work.....	51
Appendix A.....	53
Bibliography	54

List of Figures

Figure	Page
1. Artist's Concept of ABL (3).....	2
2. Phase Matching of k-vectors for FWM. (a) The Forward Geometry Can Produce Second Order Stokes. (b) The Backward Geometry Cannot Produce a k-vector of Proper Magnitude for Second Order Stokes.....	13
3. Typical Fiber Bragg Grating Reflectivity with Multimode Excitation (left) and Single Mode Excitation (right) (14).....	20
4. Diagram of the RFL Oscillator Setup. 1) Lee Pump Laser. 2) 16x Objective Lenses. 3) 300m RFL oscillator. 4) LWP Edge Filter. 5) Diagnostics.....	21
5. Edge Filter Transmission Spectra (13).	22
6. Diagram of 5.3km Fiber with Polarization Beam Splitters. 1) Lee Pump Laser (top) and CEO Pump Laser (bottom). 2) 16x Objective Lenses. 3) 10x Objective Lens. 4) 300m RFL oscillator. 5) 5.3km Fiber amplifier. 6) Flat Mirror. 7) LWP Edge Filter. 8) Diagnostics. 9) PBS Cubes. 10) $\lambda/2$ Waveplate. 11) Beam Blocks.....	24
7. Diagram of 5.3km Fiber without Polarization Beam Splitters. 1) Lee Pump Laser (top) and CEO Pump Laser (bottom). 2) 16x Objective Lenses. 3) 10x Objective Lens. 4) 300m RFL oscillator. 5) 5.3km Fiber amplifier. 6) Flat Mirror. 7) LWP Edge Filter. 8) Diagnostics.....	25
8. Diagram of 2.5km Fiber Amplifier. 1) Lee Pump Laser (top) and CEO Pump Laser (bottom). 2) 16x Objective Lenses. 3) 10x Objective Lens. 4) 300m RFL oscillator. 5) 2.5km Fiber amplifier. 6) Flat Mirror. 7) LWP Edge Filter. 8) Diagnostics.....	26
9. Diagnostic Setup for Measurements Leading to M^2 Calculation.....	28
10. Diagram of Setup for Measurement of FWM in the 5.3km Fiber. 1) CEO Pump Laser. 2) 16x Objective Lens. 3) 10x Objective Lens. 4) 5.3km Fiber amplifier. 5) Flat Mirror. 6) LWP Edge Filter. 7) Diagnostics.....	31
11. FWM in the 5.3km Fiber with only 3.5 W of Pumping.....	31
12. FWM in the 5.3km Fiber, 1.2mW of Forward Stokes Power.....	32
13. FWM in the 5.3km Fiber, Pump at 80mW over the Stokes Threshold.	32

Figure	Page
14. Backward Stokes Spectrum from the 5.3km Fiber, 10mW of Stokes.	33
15. Sensitivity of Forward and Backward Stokes Excitation with Poor Pump Alignment at High Power with the Fundamental Fiber Mode.....	34
16. Spectrum of RFL Seed.....	36
17. Second Order Stokes Wavelength of RFL Seed.	36
18. First Order Stokes Spectrum in 5.3km Fiber with $\lambda/2$ Waveplate.....	37
19. First Order Stokes Spectrum in 5.3km Fiber without $\lambda/2$ Waveplate.....	37
20. First Order Stokes Spectrum in 2.5km Fiber.	38
21. Spectrum of 5.3km Fiber with 10 W of Pump.....	39
22. Spectrum of 2.5km Fiber with 10 W of Pump.....	39
23. Second Order Stokes Wavelength of 5.3km Fiber with no Pumping.	40
24. Second Order Stokes Wavelength of 5.3km Fiber with 10 W of Pump.	40
25. Second Order Stokes Wavelength of 2.5km Fiber with no Pumping.	41
26. Second Order Stokes Wavelength of 2.5km Fiber with 10 W of Pump.	41
27. Near-field (left) and Far-field (right) Images of the CEO Pump Laser After 1 Meter of Fiber.	43
28. Far-field Images of the Stokes Beam in the 5.3km Fiber with 0 W (left) and 5 W (right) of pump.	43
29. Far-field Images of the Stokes Beam in the 2.5km Fiber with 0 W (left) and 5 W (right) of Pump.....	44
30. 2.5km Fiber Power Data.	46
31. 5.3km Fiber Power Data, 2 nd Trial.....	47

List of Tables

Table	Page
1. Single Pass Power Data (in mW) for Forward and Backward Stokes Generation in the 5.3km Fiber.	34
2. Standard Deviation of Power Measurements in Watts in 2.5km Fiber.....	47

BACKWARD AMPLIFICATION AND BEAM CLEANUP OF A RAMAN FIBER LASER OSCILLATOR USING A MULTI-MODE GRADED INDEX FIBER AMPLIFIER

I. Introduction

Background

The number of applications utilizing fiber lasers has seen a significant growth in recent years, and as a result they have become more widespread. As the technology behind them continues to mature, their capabilities will likely expand further with each passing year. One of the key areas responsible for the observed growth of these lasers is the rapid strides made in the amount of power they are capable of delivering while maintaining excellent beam quality. The possibility for high power applications opens the way for new customers to employ these lasers.

One customer interested in high power fiber lasers is the Department of Defense (DoD). The most notable DoD work with high power lasers so far is the Air Force's Airborne Laser (ABL) and the Army's Tactical High Energy Laser (THEL). Both the ABL and THEL use chemical lasers to generate the high energy beam needed to destroy their targets. However, chemical lasers are difficult to support logistically due to the necessity of transporting large quantities of specialized chemicals along with the laser. The chemicals are an unattractive limiting factor because they limit the number of shots. Also, the reaction chambers for the chemical lasing process and associated heat and chemical dissipation system tend to be bulky, further limiting the portability of these

lasers. In order to increase portability and supportability, lasers powered by electricity are desired.



Figure 1. Artist's Concept of ABL (3).

Fiber lasers offer some of the advantages that chemical lasers lack for meeting the needs of DoD. They are very compact and lightweight. Their large surface areas often enable air cooling for heat management. Semiconductor lasers using electrical power are already the standard method for optically pumping fiber lasers, providing mature techniques for coupling these devices together. Finally, both the semiconductor pump laser and fiber laser incorporate the ruggedness required by DoD for durability and transportability during deployment. If fiber lasers can also meet the desired beam quality and high power required, they would be a good fit for the next generation of DoD lasers.

The current primary user of fiber lasers, the communications industry, is not especially concerned with the maximum power a fiber laser can attain. They are much more concerned with high beam quality that can maintain its fidelity over long

transmission distances. Therefore, their research has focused almost exclusively on single-mode fibers because of the requirement to produce a high quality, unaberrated signal. Single-mode fibers use a small core in which only one transverse mode can propagate due to the size of the core. But the small core also means a small spatial gain area, limiting the output power.

Therefore, the simplest solution for increasing power output and gain in a fiber laser is to increase the size of the core by moving from single-mode to multi-mode fibers. This also allows for much more energy to be contained within the fiber without exceeding the maximum power density that the material can survive. Unfortunately, multi-mode fibers support multiple transverse modes, and as a result beam quality suffers dramatically.

However, the high power offered by multi-mode fibers must be coupled with good beam quality in order for the beam to be propagated over large or even moderate distances while still achieving a high irradiance at a potential target. Without high beam quality to accompany the high power, the DoD cannot exploit the other benefits of fiber lasers.

Recently, new techniques have emerged that may present a solution to this problem of trading power for quality. A nonlinear process known as Stimulated Raman Scattering (SRS) has shown definite beam clean-up qualities at high intensities. Utilizing the SRS conversion process, it is possible to dramatically improve a highly aberrated high power beam. Many methods are being investigated to optimize this conversion process, seeking to simultaneously maximize output power and beam quality.

Research Objectives

Several recent experiments have attempted to optimize the SRS conversion process, particularly in terms of power conversion, amplification, and degree of beam cleanup. However, a significant hindrance has been encountered due to another nonlinear process known as Four Wave Mixing (FWM). Using a forward pumped amplifier, FWM causes higher order SRS frequencies to appear prematurely. The result is that even modest powers create output consisting of multiple discrete widely-spaced frequencies instead of the desired single frequency.

The objective of this research is to demonstrate that FWM can be eliminated by using a backward pumping geometry. However, for SRS to remain a viable option for use in brightness and power scaling for the DoD, it must also retain its ability to amplify the input beam in this configuration and improve the beam's quality.

Summary

This chapter reviewed the background surrounding the interest in high power lasers by the DoD. The need for a more maintainable solution is generating interest in solid-state lasers and particularly fiber lasers due to their recent rapid progress in maximum power output. Newly emerging techniques like SRS are being explored for possible use in furthering the capabilities of fiber lasers. Currently, FWM presents a barrier to power scaling and backward amplification is presented as a possible solution. The objectives of eliminating FWM while preserving amplification and beam cleanup were presented.

Preview

Chapter two focuses on the basics of nonlinear optics and the processes of SRS and FWM as they apply to this research effort. The important physics governing SRS in fibers is covered and the recent relevant research is reviewed.

Chapter three covers the setup for the various experiments performed. The types of equipment used, and methods of measurements taken are then detailed.

Chapter four presents the results of the experiments and an analysis of the data. To evaluate the presence of FWM, data is presented on the spectrum of the amplifier output. Then, beam profile and beam quality measurements are examined in order to assess beam cleanup. Last, power measurements are reviewed to evaluate the amount of gain and amplification produced.

Chapter five concludes the findings presented in chapter four and presents some possible avenues for future research.

II. Literature Review

Chapter Overview

This chapter reviews the physics relevant to this research project and its experiments. First is an introduction to the concept of nonlinear optics. Then the two areas of nonlinear optics are discussed that apply to this research, SRS and FWM. Next are the various relevant equations and physics covering SRS and light propagation in a fiber. Finally reviewed is the relevant research leading up to this project.

Introduction to Nonlinear Optics

Linear optics is the realm of physics enjoyed by the interaction of light and matter except in the presence of very strong electric fields. Before the advent of the laser, such strong electric field strengths were encountered relatively rarely. However, since the birth of the age of lasers in 1961 with Maiman's ruby laser (15:351,434), the field of nonlinear optics has developed into a fully recognized regime of light/matter interactions.

In the field of linear optics the interaction of an electric field with matter is described by

$$\vec{P}(t) = \chi^{(1)} \vec{E}(t) \quad (1)$$

where $\vec{E}(t)$ is the electric field, $\chi^{(1)}$ is the linear electric susceptibility of the material, and $\vec{P}(t)$ is the polarization of the material (4:2). This induced polarization of the atomic

dipoles in the material is responsible for reflection, and refraction—both well studied, and part of the basic foundation of optics.

However, in the presence of a very strong electric field, the response of a material ceases to be linear. The atomic dipoles can no longer oscillate fast enough to stay in phase and maintain the frequency of the exciting electromagnetic field (the light). As a result, they set up a second field in the material which in turn interacts with the propagating excitation field. In order to treat this, Eqn. (1) can be expanded as a power series as seen in Eqn. (2) below.

$$\vec{P}(t) = \chi^{(1)} \vec{E}(t) + \chi^{(2)} \vec{E}^2(t) + \chi^{(3)} \vec{E}^3(t) + \dots \quad (2)$$

Again, $\vec{E}(t)$ is the electric field, $\chi^{(1)}$ is the linear electric susceptibility of the material, and $\vec{P}(t)$ is the polarization of the material. But now, $\chi^{(2)}$ is the quadratic susceptibility and $\chi^{(3)}$ is the cubic susceptibility, etc (4:2). These higher order susceptibilities are present in many materials, but because they are much smaller than the linear coefficient, they are not observed until a sufficiently high electric field is present to allow them to make a significant contribution to the polarization. These second and third order terms can allow new frequencies to appear that are different from the exciting field and are responsible for a host of phenomena like the Pockels effect, Kerr effect, stimulated Brillouin scattering, stimulated Raman scattering, Four-Wave Mixing, and many others. Of these, SRS and FWM are both very important to the work presented in the following chapters and deserve a more detailed discussion.

Stimulated Raman Scattering (SRS).

SRS is a third-order nonlinear effect. SRS begins as a spontaneous noise phenomenon as a result of the exciting field, but the process builds on itself and can experience gain until a considerable amount of the exciting field's energy is converted. Raman scattering is a scattering interaction between a pump photon and a vibrational state of the molecules of the material. The pump photon excites a virtual energy level in the molecule. The molecule then emits a Stokes photon and decays to an allowed excited vibrational state. Although the reverse can also occur (a pump photon excites an excited vibrational state to a virtual state, then decays to the ground state emitting an anti-Stokes photon), the Boltzmann distribution for occupied energy states dictates that this process is several orders of magnitude smaller. Mathematically the conservation of energy during Raman scattering is expressed by

$$\omega_s = \omega_L - \omega_v \quad (3)$$

where ω_L is the laser pump frequency, ω_v is the vibrational frequency of the molecule, and ω_s is the difference between the pump and vibrational frequencies, or Stokes frequency.

Spontaneous Raman scattering is a fairly weak process and isotropic. SRS on the other hand, tends to be very strong and creates a narrow cone in both the forward and backward directions. It is possible to investigate the relation between these processes through an equation such as

$$P_s = \frac{dm_s}{dt} = Dm_L(m_s + 1) \quad (4)$$

where P_s represents the probability per unit time that a photon will be emitted into Stokes mode S , D is a material proportionality constant, m_L is the mean number of photons per mode of the laser, and m_s is the mean number of photons in Stokes mode S . Manipulating this for a z spatial evolution yields

$$\frac{dm_s}{dz} = \frac{1}{c/n} Dm_L(m_s + 1) \quad (5)$$

Here, c is the speed of light and n is the index of refraction of the material. In the limit that $m_s \ll 1$, the solution of Eqn. (5) is

$$m_s(z) = m_s(0) + \frac{1}{c/n} Dm_L z \quad (6)$$

where $m_s(0)$ is the input Stokes photon occupation. This limit represents the case of spontaneous Raman scattering and increases linearly with propagation in z . But, when $m_s \gg 1$, the solution of Eqn. (5) becomes

$$m_s(z) = m_s(0)e^{\frac{Dm_L}{c/n}z} \quad (7)$$

where exponential growth now occurs in z . This second limit represents the process of SRS (4:452-455).

In terms of the polarization, the equation that gives rise to the Stokes frequency, $P(\omega_s)$, for a wave propagating in z is given by

$$P(\omega_s) = 6\chi^{(3)}(\omega_s = \omega_s + \omega_L - \omega_L) |A_L|^2 A_s e^{ik_s z} \quad (8)$$

where again ω_s is the Stokes frequency, ω_L is the laser frequency, $\chi^{(3)}$ is the third order susceptibility of the material, A_L is the laser amplitude coefficient, A_s is the Stokes amplitude coefficient, and k_s is the wave vector of the Stokes wave. For those interested in the full development and origin of the above equation, Boyd covers this completely in his book (4:70, 419, 460-462).

Classically, the molecular vibration of SRS can be explained as a consequence of a beat frequency between the exciting field and the Stokes field. If the polarizability of the material depends on the internuclear distance of the molecule, it varies in time as the molecule vibrates. This creates sidebands in the laser frequency at $\pm \omega_v$. Eqn. (3) showed this to be the Stokes frequency. Now, frequency mixing between the laser and Stokes frequencies creates

$$\omega_v = \omega_L - \omega_S \quad (9)$$

Basically, a sufficient number of Stokes photons beating with the exciting field can generate a resonance in the vibrational state. The exciting field then is modulated by the vibrating index of refraction such that more Stokes photons are generated, which enhances the resonance, which generates more photons. This allows for gain at the Stokes frequency, and if the first order Stokes frequency meets the threshold condition (gain exceeds loss), it can generate its own Stokes photons, also called second order Stokes, etc. (4:459-460).

Four Wave Mixing (FWM).

FWM is also a third-order nonlinear effect. It occurs when a phase matching condition is met between the frequencies present in the material. The combination of three different frequencies creates a fourth frequency by adding or subtracting. This condition is expressed by the following equations

$$\vec{k}_4 = \pm \vec{k}_1 \pm \vec{k}_2 \pm \vec{k}_3 \quad (10)$$

$$\omega_4 = \pm \omega_1 \pm \omega_2 \pm \omega_3 \quad (11)$$

where \vec{k}_i and ω_i are the i^{th} different k-vector and frequency components combining to generate a fourth frequency. These components can be the same (degenerate) or different from each other, but both equations must be satisfied simultaneously.

A specific example of FWM of interest is shown below in

$$\omega_{s_2} = \omega_{s_1} + \omega_{s_1} - \omega_p \quad (12)$$

where ω_p is the pump frequency, ω_{s_1} is the first order Stokes frequency, and ω_{s_2} is the second order Stokes frequency. In a forward pumping geometry, Figure 2a below shows that the phase matching condition in the direction of propagation can be met for the combination of pump and first order Stokes frequencies needed to produce the second order Stokes frequency. Thus, second order Stokes appears from FWM without the first order Stokes reaching the threshold condition. Similarly, Eqn.(13) shows that second order Stokes and first order Stokes can combine through FWM to generate third order Stokes, etc.

$$\omega_{s_3} = \omega_{s_2} + \omega_{s_1} - \omega_{s_1} \quad (13)$$

The final outcome is a run-away cascade of Stokes orders present in the output beam.

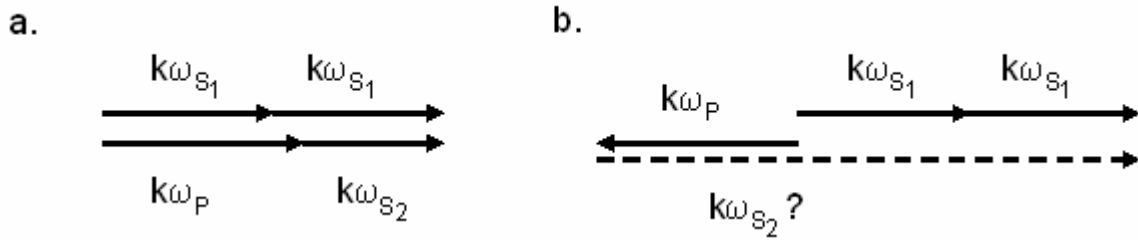


Figure 2. Phase Matching of k-vectors for FWM. (a) The Forward Geometry Can Produce Second Order Stokes. (b) The Backward Geometry Cannot Produce a k-vector of Proper Magnitude for Second Order Stokes.

However, in the backward geometry, Figure 2b above shows that the combination of frequencies that generate a second order Stokes frequency cannot also produce the k-vector of proper magnitude for second order Stokes. In reality, $k\omega_{S_2}$ has a magnitude that is very close to the magnitude of $k\omega_{S_1}$, but the backward geometry would require a magnitude almost three times that of $k\omega_{S_1}$ to phase match. Therefore, this combination of FWM is forbidden for the backward geometry. It is important then to explore the backwards geometry to avoid the run-away cascade of frequencies caused by FWM.

Physics of Fibers and Nonlinear Optics

In order to work with fibers there are a number of important parameters and interactions that are vital to understand. The performance characteristics of a fiber include the acceptance angle of the fiber or numerical aperture (NA), the core diameter, and the attenuation of the fiber - usually given in dB/km.

The fiber NA is a measure of the maximum divergence angle of light entering the fiber that will be guided down the fiber (12:25). Fiber NA depends on the difference in the refractive indices of the core and the cladding in the fiber. The NA is a key factor in

deciding the size of objective lens to use when coupling light into the fiber. Trade-offs are necessary, since a stronger objective lens will make a smaller spot, but the spot will be diverging faster. If the spot diverges faster than the fiber NA, most of the light will not be guided through the fiber core and will end up in the cladding. However, a weaker objective lens may fail to focus the light to a spot as small as the core of the fiber, again leaving significant power in the cladding. This reveals the difficulty in coupling high-power beams into fibers, since a misaligned beam, one with too large of a spot size, or one that is not well matched to the fiber NA, will couple a lot of the power into the cladding of the fiber and cause the tip to burn.

The attenuation of the fiber is important to understand, since, in a long fiber, much of the power may be absorbed during transmission. The attenuation depends on the wavelength, and for multimode fibers usually must be measured (7). The conversion of the fiber attenuation to a loss per length α_p is given by

$$\alpha_{\text{dB}} = -\frac{10}{L} \log \left(\frac{P_T}{P_0} \right) = 4.343\alpha_p \quad (14)$$

where α_{dB} is the attenuation in dB/km, P_T is the power transmitted through the fiber and P_0 is the power coupled into the fiber (1:6). From α_p and L , the length of the fiber, it is possible to calculate the effective length of the fiber, L_{eff} , using the relationship below

$$L_{\text{eff}} = [1 - \exp(-\alpha_p L)] / \alpha_p \quad (15)$$

The effective length is the length of gain equivalent to a fiber with no attenuation of the pump (1:301). The gain from a Raman fiber amplifier, G_A , is then given by

$$G_A = \exp(g_R P_0 L_{\text{eff}} / A_{\text{eff}}) \quad (16)$$

where g_R is the Raman gain factor of the material, P_0 is the pump power coupled into the fiber, and A_{eff} is the effective area of the core of the fiber (1:312). The effective area is a particularly difficult quantity to compute, given below by

$$A_{\text{eff}} = \frac{\left(\int_{-\infty}^{\infty} \int_{-\infty}^{\infty} |F(x, y)|^2 dx dy \right)^2}{\int_{-\infty}^{\infty} \int_{-\infty}^{\infty} |F(x, y)|^4 dx dy} \cong \pi w^2 \quad (17)$$

where $F(x, y)$ is a modal distribution over the fundamental fiber modes. However, this function is usually approximated by a Gaussian distribution and then yields the much simpler relationship on the right (1:44). For the fiber used in this research, the width factor w can be determined from the numerical approximation (8:2023)

$$w = a \left(\sqrt{\frac{2}{V}} + \frac{0.23}{V^{\frac{3}{2}}} + \frac{18.01}{V^6} \right) \quad (18)$$

where a is the radius of the fiber core and V is the normalized frequency given by

$$V = ak_0NA \quad (19)$$

where again a is the radius of the fiber core and k_0 is the wavenumber.

From these equations it was possible to calculate the A_{eff} of the 50 μm fibers used in this research and was found to be approximately 131 μm^2 . Knowing that the typical value used for the Raman gain factor g_R for silica fibers is approximately 1×10^{-13} m/W, it is then possible to use

$$P^{th} \approx \frac{20A_{\text{eff}} p_{\text{fac}}}{g_R L_{\text{eff}}} \quad (20)$$

to make a threshold calculation for SRS in the backward geometry (1:312). Here, p_{fac} is a factor between 1 and 2 that depends on whether polarization is maintained in the fiber between the pump and the Stokes waves. For the longer fiber, P^{th} was found to be as low as 8.5 W if polarization is maintained, while the shorter fiber had a calculated minimum threshold of 13 W. For this reason, a seed will be used since this threshold will probably not be met and there is nothing to cause a constant polarization relationship in the fiber.

Finally, it is important to mention that the Raman shift for silica fibers is approximately 13 THz. Starting from 282 THz (1.064 μm), our frequencies of interest are 269 THz (1.1165 μm) for first order Stokes, and 256 THz (1.1723 μm) for second order Stokes.

Relevant Research

In 1992, a paper by Chiang examined SRS in a 50 μm graded index fiber (5). In it, he details a discovery that although the fiber is multimode, the low order propagation modes are favored by the generated Stokes beam and so the fiber can simulate a single-mode fiber or low order multimode fiber. The suggestion was then made that the larger core size of the fiber would allow a larger spot size (allowing more power transmission without exceeding material damage thresholds), and more power for a Raman laser, but still propagate in a low order mode (better beam quality) due to the preferential excitation of the fundamental mode.

A later experiment exploring backward SRS for wavefront reconstruction (WFR) found less WFR than expected (6). WFR relies on a large number of Raman modes for cross correlation with the pump in order to accomplish its phase conjugation.

Remembering Chiang's work, the authors surmised that fewer Raman modes were present in the fiber than they had expected.

Russell, *et al* experimented with forward SRS in order to characterize its potential for beam cleanup (11). During their experiments, FWM was found to significantly limit the power at a single frequency in the Stokes output. However, their results also

suggested the SRS conversion process could potentially improve beam quality by more than an order of magnitude over the quality of the pump.

2004 saw the publication of a paper from Baek and Roh wherein a pump beam with an M^2 of approximately 7.0 produced a Stokes beam with an M^2 of 1.66 by implementing SRS cleanup in a Raman fiber laser oscillator configuration (2). This improvement was possible because of the beam cleanup properties identified in the previous papers.

Summary

This chapter began with a basic introduction to nonlinear optics. In the introduction, the relevant processes of SRS and FWM were discussed. Next, the physics and equations applicable to SRS in a fiber were examined. Finally, the previous research that led up to this research project was reviewed.

III. Methodology

Chapter Overview

The purpose of this chapter is to explain the approach and setup used in each of this project's experiments. The setup for each experiment is explained as well as the key aspects in which it differs from the other experiments. The setup for the Raman Fiber Laser (RFL) oscillator is explained first since it is used to produce the initial Stokes seed used by each of the experiments. Also included in this section is a discussion of the cavity constructed for the pump laser used to pump the amplifiers. Next described is the first setup using the 5.3km fiber with a $\lambda/2$ waveplate and polarization beam splitting cubes to control the power. Then, the second configuration of the 5.3km fiber is explained. Following that, the setup for the testing of the 2.5km fiber is covered. Finally, a description is provided of the diagnostic equipment used and types of measurements taken.

Raman Fiber Laser Oscillator and Pump Laser Cavity

The original design for the experiments involved using a powerful Cutting Edge Optonics (CEO) diode pumped Nd:YAG laser head as both the pump for the RFL oscillator and the fiber amplifier. However, the poor beam quality (high M^2) of the CEO when operating at a power sufficient to allow splitting into two channels precluded efficient coupling into the 50 μm fibers. This approach was abandoned in favor of using

two lasers: the CEO laser for pumping the fiber amplifier and a diode pumped Nd:YAG Lee laser for pumping the RFL.

The fiber oscillator was constructed using a 300 meter fiber with a 50 μ m diameter multimode fiber core. The fiber was manufactured by Corning, and was a graded index Corguide fiber with 125 μ m cladding and 245 μ m buffer. The fiber is a silica fiber doped with Germanium to create the index gradient and has an acceptance angle of 0.20 NA.

Fiber Bragg gratings manufactured by Avensys were spliced onto both ends of the fiber to create a cavity for the first order Stokes wavelength at 1.1165 μ m. In order to maximize the amount of Stokes generation in the cavity, gratings rated at 99% reflectivity by Avensys were chosen for both ends. (The intent here was to ensure a seed rather than maximize the amount of seed generated.) However, recent in-house assessments of these rated reflectivities suggest their performance may only be valid for single mode fiber (see Figure 3 below), and that for the case of a multimode fiber, actual reflectivity of these gratings is probably not higher than 50%.

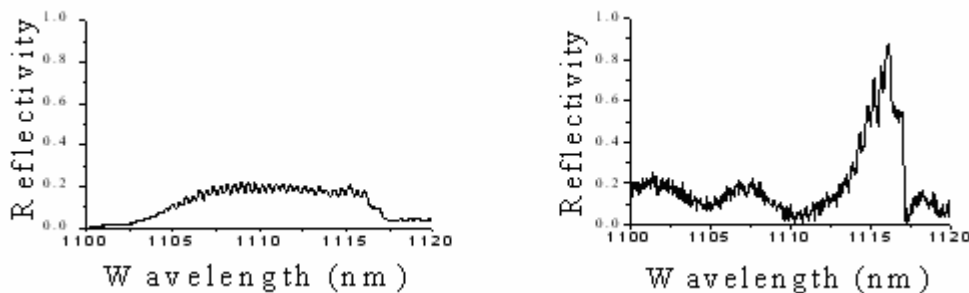


Figure 3. Typical Fiber Bragg Grating Reflectivity with Multimode Excitation (left) and Single Mode Excitation (right) (14).

The Lee laser at $1.064\mu\text{m}$ was used to pump the fiber oscillator on one end, and the output at $1.1165\mu\text{m}$ from the oscillator was then passed through an Edge Filter to separate the Stokes and the residual pump light. This is shown in Figure 4 below. The Edge Filter was manufactured by Semrock and is a Long Wave Pass (LWP) filter that reflects light at $1.064\mu\text{m}$, but transmits longer wavelengths like $1.1165\mu\text{m}$. The transition from near total reflection to near total transmission is very abrupt as can be seen in Figure 5 on the next page.

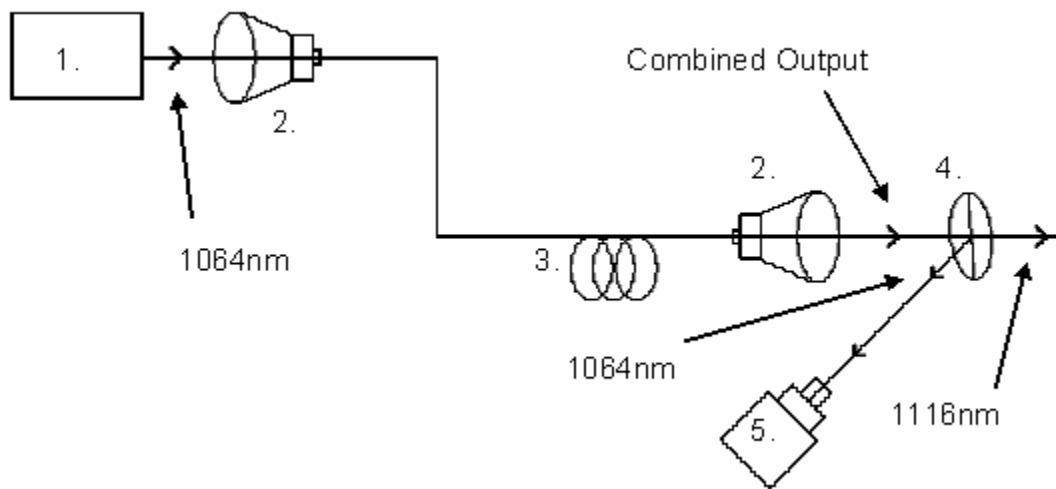


Figure 4. Diagram of the RFL Oscillator Setup. 1) Lee Pump Laser. 2) 16x Objective Lenses. 3) 300m RFL oscillator. 4) LWP Edge Filter. 5) Diagnostics.

A diode pumped CEO laser head was used to pump the fiber amplifier for each of the experiments. Using the manufacturer specifications as a guide, two flat mirrors were selected to create the cavity: one 99% high reflectivity mirror and one 80% reflectivity mirror for the output coupler. The distance between the two mirrors was approximately

28cm with the laser head centered between the mirrors. This produced a maximum output power in excess of 115 W when supplying the maximum diode current of 22 Amps.

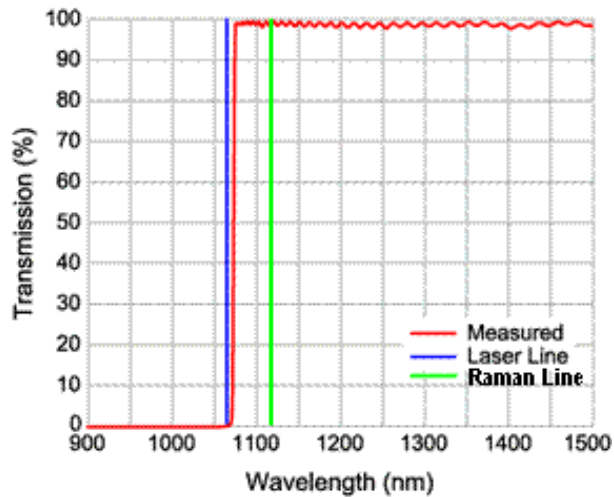


Figure 5. Edge Filter Transmission Spectra (13).

Later, an adjustable iris aperture was inserted into the cavity just before the output coupler to improve the beam quality of the pump output in order to achieve an acceptable coupling efficiency with the 50 μ m fiber. Due to the very small aperture size needed to accomplish this, the reduced maximum output power was approximately 12 W.

The Lee laser had a co-propagating Helium Neon (HeNe) laser operating in the visible range at 632.8nm that was used to assist with aligning the infrared output of the YAG. To assist with alignment of the CEO laser, a second HeNe laser operating at 548nm was positioned behind the high reflectivity mirror and used to align the cavity and output of the CEO.

Experiment 1: 5.3km Fiber with Polarization Beam Splitters

The first fiber tested for the amplifier was a 5.3km length of Corning 50 μ m diameter multimode fiber core. The fiber was a graded index Corguide fiber with 125 μ m cladding and 450 μ m buffer. The fiber was a much older product (1992) and some of the details of its specifications have been lost, but with the exception of the unusual buffer diameter and age, exhibited characteristics identical to the standard fiber used in the oscillator.

The amplifier was placed after the Edge Filter with the Stokes output of the RFL entering the front end of the amplifier. The output of the CEO laser pump was passed through a Polarization Beam Splitting (PBS) cube in order to create a polarized beam while dumping the other polarization. It was then passed through a $\lambda/2$ plate and then through a second PBS cube. This allowed the CEO diodes to be run at full power continuously, and the amount of power supplied to be adjusted by rotating the $\lambda/2$ plate. The beam was then reflected from a mirror and then a second Edge Filter into the back end of the amplifier. Diagnostics for measuring the output of the amplifier were placed behind the second Edge Filter. Figure 6 below shows this setup.

One of the key advantages for this setup was being able to control power using the $\lambda/2$ plate. This allowed alignment to be made using the fully aberrated high power beam of the pump while transmitting only a fraction of the total power to the fiber mount. This helped prevent burning the fiber tip during the alignment process.

The main disadvantage for this setup was that half the power (one polarization) was lost and only about 5 W of power was available for pumping the amplifier.

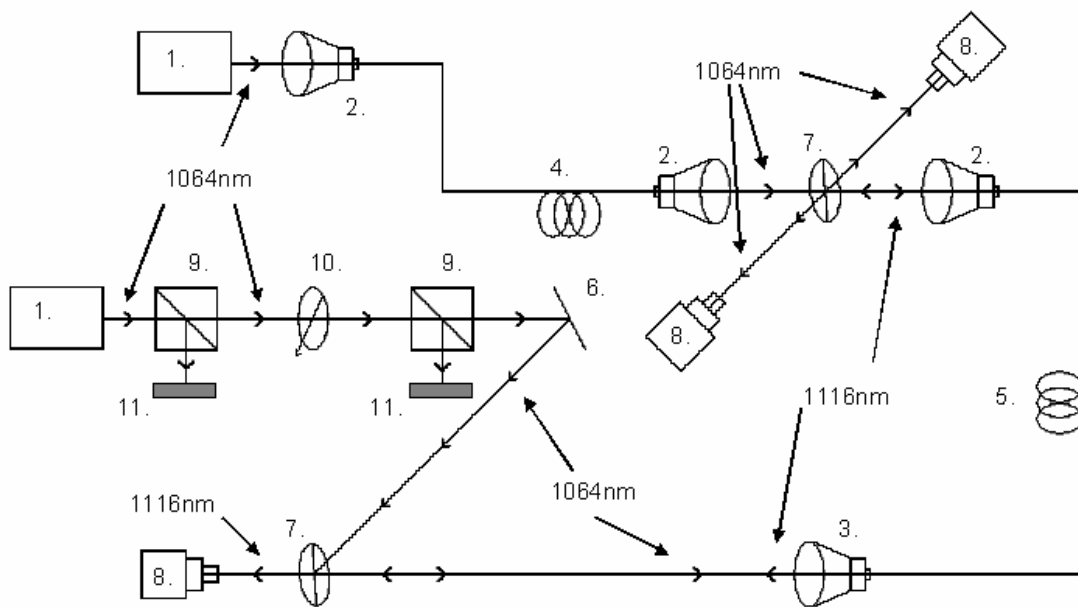


Figure 6. Diagram of 5.3km Fiber with Polarization Beam Splitters. 1) Lee Pump Laser (top) and CEO Pump Laser (bottom). 2) 16x Objective Lenses. 3) 10x Objective Lens. 4) 300m RFL oscillator. 5) 5.3km Fiber amplifier. 6) Flat Mirror. 7) LWP Edge Filter. 8) Diagnostics. 9) PBS Cubes. 10) $\lambda/2$ Waveplate. 11) Beam Blocks.

Experiment 2: 5.3km Fiber without Polarization Beam Splitters

The second configuration used for testing was identical to the one used in the first experiment except that the PBS cubes and $\lambda/2$ waveplate were removed. Figure 7 below shows this arrangement.

An advantage for this arrangement is that since neither polarization from the pump is discarded, higher power is available for pumping the fiber. The power delivered by the CEO pump laser is controlled by setting the power supplied to the diodes pumping the YAG rod.

However, this means that alignment of the fiber at high powers becomes very difficult since even a small adjustment away from the optimum can cause the fiber to

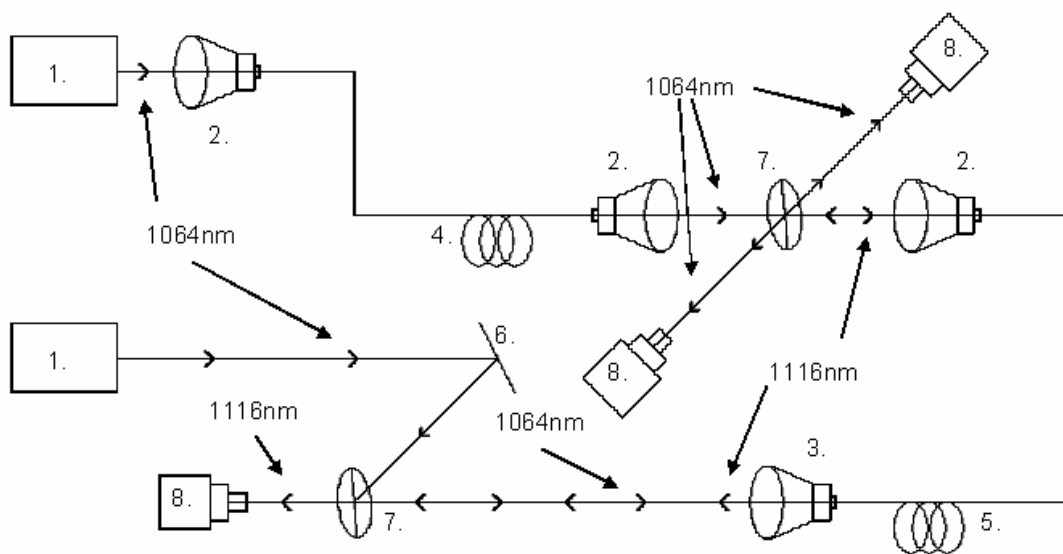


Figure 7. Diagram of 5.3km Fiber without Polarization Beam Splitters. 1) Lee Pump Laser (top) and CEO Pump Laser (bottom). 2) 16x Objective Lenses. 3) 10x Objective Lens. 4) 300m RFL oscillator. 5) 5.3km Fiber amplifier. 6) Flat Mirror. 7) LWP Edge Filter. 8) Diagnostics.

burn. This disadvantage is significant, since the beam profile of the pump changes at high power due to the presence of higher order transverse modes, and adjustments to locate the optimum alignment at high power are needed. At some point, a trade-off must be made between continuing to look for the optimum fiber alignment and thereby risking burning the fiber, versus accepting a working alignment that does not burn the fiber at full power, but is also not the optimum alignment. After many attempts to align at high powers, 7 W was chosen as the highest power practical to attempt adjustments, although pump power up to 10 W was achieved.

Experiment 3: 2.5km Fiber Amplifier

The second fiber tested for the amplifier was a 2.5km length of Corning 50 μ m diameter multimode fiber core. The fiber was a graded index Corguide fiber with 125 μ m cladding and 245 μ m buffer. This fiber was identical in specifications to the 300m fiber used for the RFL oscillator. The setup for this experiment is shown below in Figure 8. It is identical to the setup in Experiment 2, except for the only change being a different fiber used for the amplifier segment.

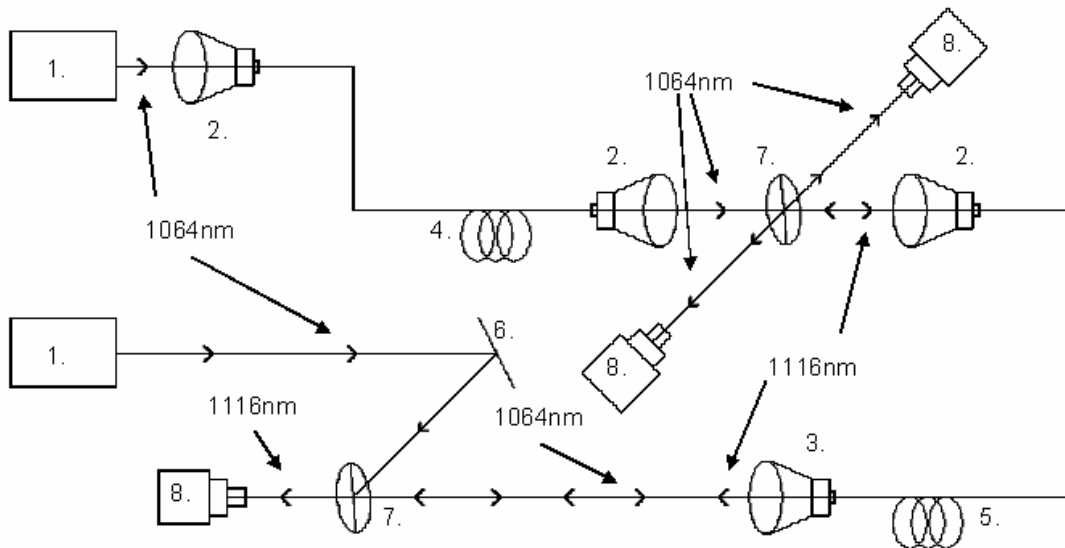


Figure 8. Diagram of 2.5km Fiber Amplifier. 1) Lee Pump Laser (top) and CEO Pump Laser (bottom). 2) 16x Objective Lenses. 3) 10x Objective Lens. 4) 300m RFL oscillator. 5) 2.5km Fiber amplifier. 6) Flat Mirror. 7) LWP Edge Filter. 8) Diagnostics.

The advantages and disadvantages to this setup are the same as Experiment 2, since only the choice of fiber for the amplifier was changed. The shorter fiber used for

the amplifier means less expected attenuation of the RFL seed beam, but also a shorter gain length.

Diagnostic Equipment Description

Data was collected in each of the three experiments in three main areas: spectral data, beam profile and beam quality measurements, and power measurements.

The spectral data was collected using an Ando AQ 6315 B Optical Spectrum Analyzer. Data sets were collected on the spectrum of the RFL seed, and on the output Stokes beam from each of the fiber amplifier configurations. The amplifier datasets were collected for three different levels of pumping: 0 W, 5 W, and 10 W.

Each data set consisted of three spectral captures: one showing the first order Stokes frequency, one showing the second order Stokes frequency, and one broadband image covering the pump, first order, and second order frequencies together. The narrowband image of the first order Stokes wavelength covered from 1110nm to 1120nm with a 0.05nm high spectral resolution. The second order Stokes wavelength also used a 10nm span from 1168nm to 1178nm at this same resolution. The broadband image used a resolution of 1nm and covered from 1050nm to 1200nm.

An Alpha NIR infrared camera was used to record images of the beam profile. This camera was connected to a computer running Digital Beam Profiler software from Photon Inc. Measurements of M^2 were accomplished by scanning the camera through a secondary waist created by a 300mm lens and measuring the extent of the beam diameter. A diagram of this diagnostic setup appears in Figure 9 below. The software was using the second moment method as the definition of the beam diameter and took the average

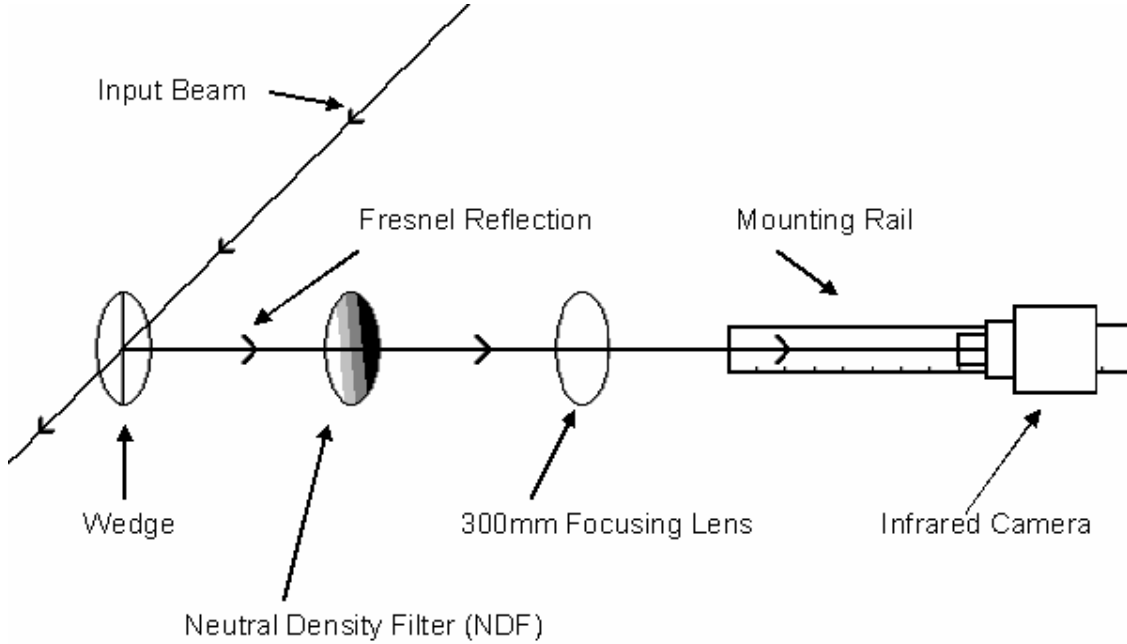


Figure 9. Diagnostic Setup for Measurements Leading to M^2 Calculation.

of 100 samples when generating this measurement. Mathematica was then used to fit these measurements to the equation of a Gaussian beam shown below

$$w_R(z) = w_{0R} \left[1 + \left(\frac{z\lambda M^2}{\pi w_{0R}^2} \right)^2 \right]^{1/2} \quad (21)$$

using a nonlinear regression technique in order to calculate a value for M^2 . In the equation, w_{0R} is the radius of the beam waist, z is the position along the direction of propagation, $w_R(z)$ is the radius of the beam at z , and λ is the wavelength of the propagating beam (10). The code used for Mathematica is given in Appendix A. Beam

profiles and M^2 measurements were performed for the RFL seed, output of each amplifier for 0 W, 5 W, and 10 W of pump, and of the seed and pump after being coupled through 1 meter of fiber. The power readings were recorded by a 30W detector head connected to a Thor Labs power meter and a 10W detector head connected to a second Thor Labs power meter. A 300 W Newport 818P-300-55 detector connected to a Newport 1825-C power/energy meter was used to monitor the residual pump from the Lee laser generating the RFL seed. Power readings for each amplifier were recorded using the Thor Labs built-in averaging ability over 1 minute intervals because the RFL seed exhibited some fluctuation over the course of a dozen seconds. The fluctuation in the seed was possibly a consequence of mode competition due to the use of multimode gratings in the RFL. Power data was also collected after 1 meter of fiber on each end of the amplifier in order to show what was actually coupled into the fiber from the pump and RFL seed.

Summary

This chapter covered the setup used to assess the feasibility of a backward seeded Raman fiber amplifier to eliminate FWM and still provide amplification and beam cleanup. To start, the setup of the RFL oscillator for generating a Raman seed and cavity for the CEO pump head was covered. Next, a description of the first setup, using the 5.3km fiber making use of a $\lambda/2$ waveplate for power control, was provided. Then, the second—more powerful—setup for the 5.3km fiber was described. After that, the setup for the testing of the 2.5km fiber was delineated. Finally, a description of the diagnostic equipment used and the types of measurements recorded was detailed.

IV. Analysis and Results

Chapter Overview

This chapter presents the data and results of the three experiments: the 5.3km amplifier with $\lambda/2$ waveplate, 5.3km without $\lambda/2$ waveplate, and 2.5km amplifier. A look at FWM and single pass unseeded Raman output is discussed first. Second, the spectral data acquired is presented and reviewed. Next, the beam profile and measurements of M^2 is covered. Finally, the amount of power output of the amplifiers is evaluated.

FWM Data

The primary reason for using the backward pumping geometry was to determine if it would eliminate the phase matching condition between the pump and the Stokes photons needed to produce FWM while at the same time producing beam cleanup. During the experiments, it was noted that the 5.3km fiber was long enough to reduce the threshold for SRS sufficiently for the generation of a weak Stokes beam in both the forward and backward directions without a seed. A full description and presentation of this data is presented here and the setup for this configuration is shown below in Figure 10.

A full set of power characterization data and several spectral images on these Stokes beams generated without a seed were collected. Both a forward propagating (as seen from the CEO pump) and a backward propagating Stokes beam were detected simultaneously during these measurements. FWM was immediately evident in the

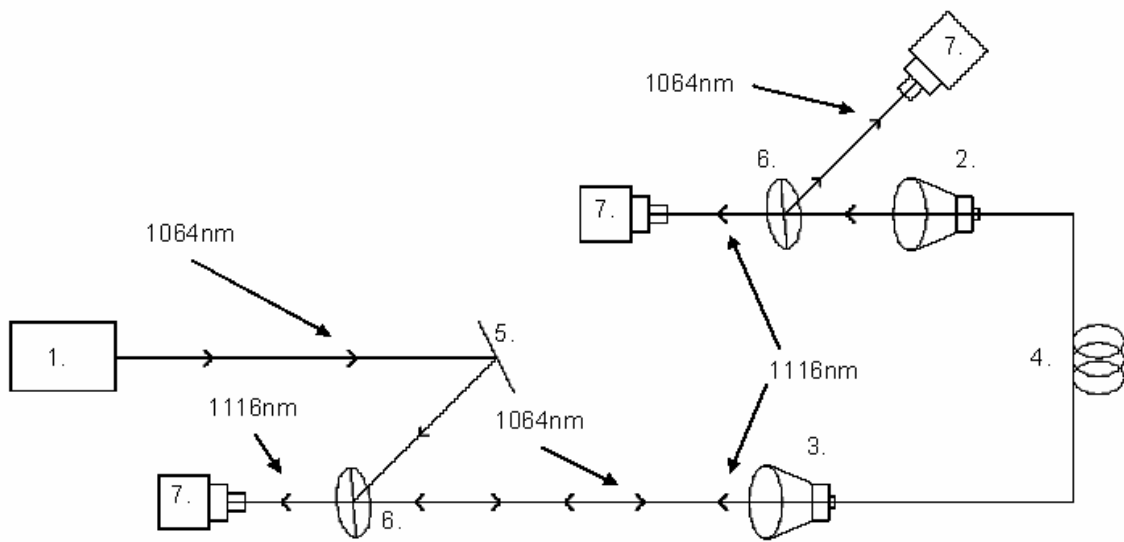


Figure 10. Diagram of Setup for Measurement of FWM in the 5.3km Fiber. 1) CEO Pump Laser. 2) 16x Objective Lens. 3) 10x Objective Lens. 4) 5.3km Fiber amplifier. 5) Flat Mirror. 6) LWP Edge Filter. 7) Diagnostics.

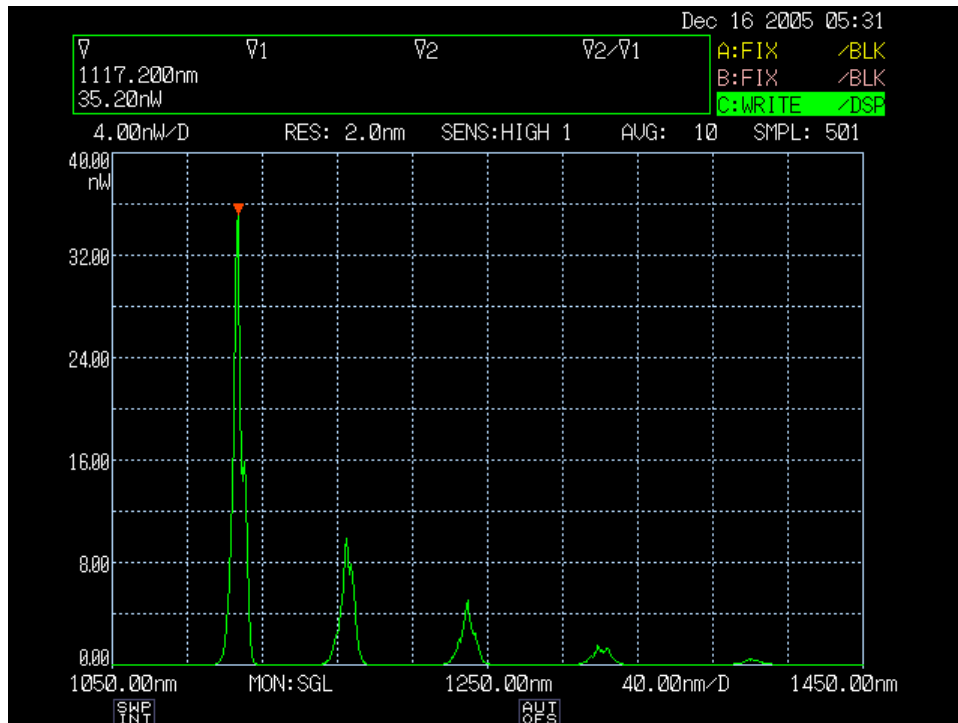


Figure 11. FWM in the 5.3km Fiber with only 3.5 W of Pumping.

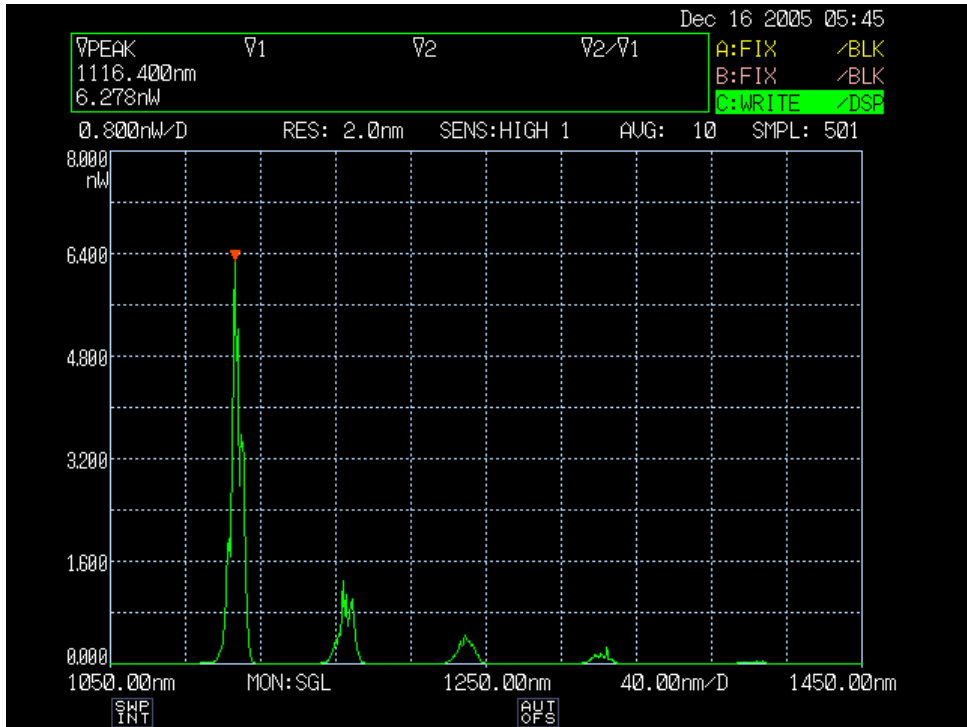


Figure 12. FWM in the 5.3km Fiber, 1.2mW of Forward Stokes Power.

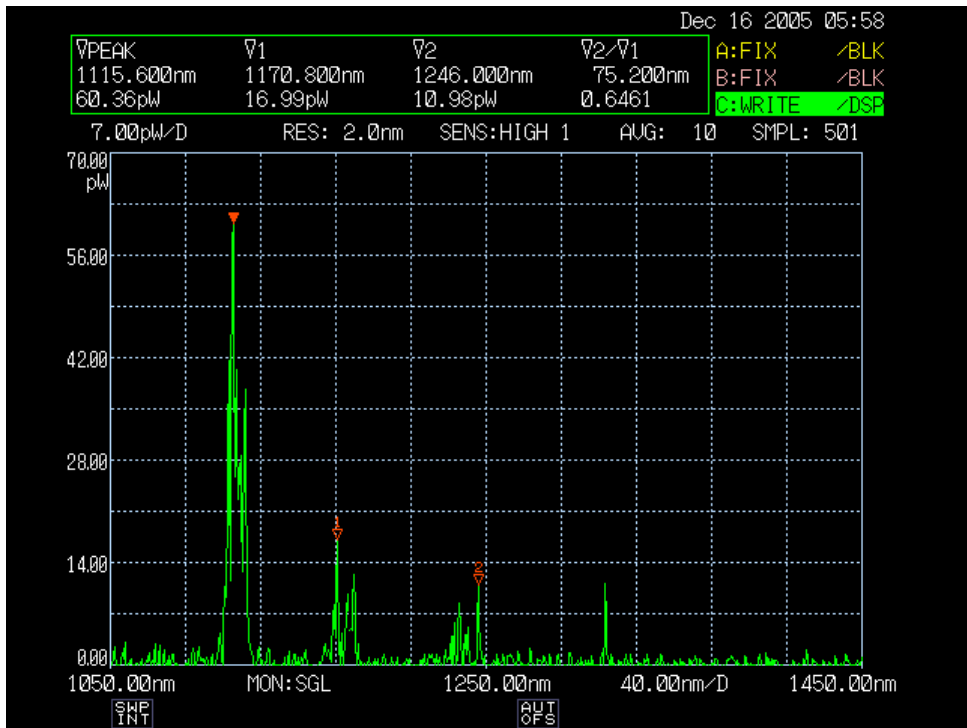


Figure 13. FWM in the 5.3km Fiber, Pump at 80mW over the Stokes Threshold.

spectral data for the forward Stokes beam and can be seen in Figure 11 and Figure 12 above.

Figure 13 above shows that the higher order Stokes modes in the forward direction are produced almost immediately. Since there is not enough power in the first order Stokes beam to reach the threshold for the second order Stokes (and similarly for the second order to start the third), they are started from FWM.

However, Figure 14 below shows the spectrum of the backward Stokes radiation. In contrast to the forward Stokes, almost all of the power exists in the first order Stokes frequency, and second and third order Stokes exist only as low level spontaneous noise.

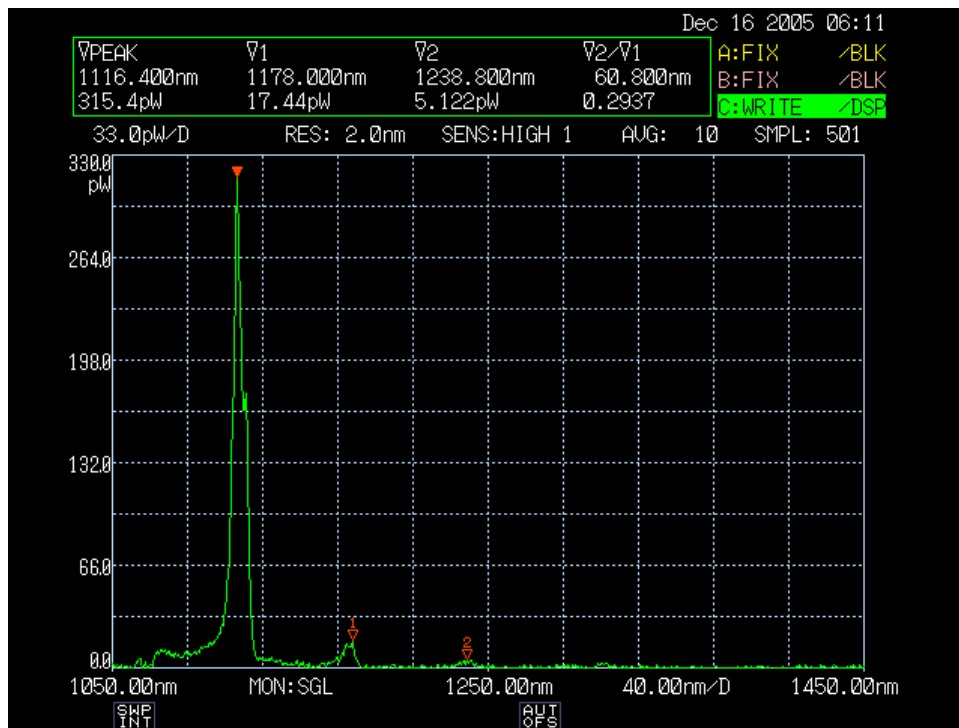


Figure 14. Backward Stokes Spectrum from the 5.3km Fiber, 10mW of Stokes.

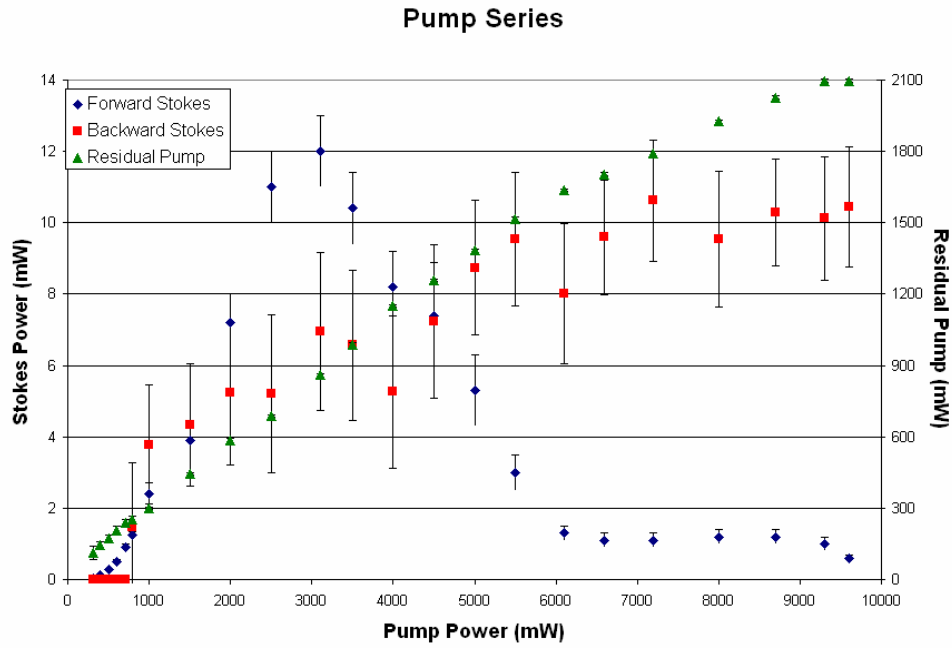


Figure 15. Sensitivity of Forward and Backward Stokes Excitation with Poor Pump Alignment at High Power with the Fundamental Fiber Mode.

Table 1. Single Pass Power Data (in mW) for Forward and Backward Stokes Generation in the 5.3km Fiber.

Pump	Forward Stokes	Error	Backward Stokes	Error	Residual Pump	Error
		Forward		Backward		Residual
310	0.02	0	0	0	112.4	26.06
400	0.11	0.01	0	0	142.9	16.84
500	0.28	0.02	0	0	173.6	15.13
600	0.5	0.05	0	0	206.7	18.55
715	0.9	0.1	0	0	237.9	15.75
795	1.25	0.1	1.476	1.788	251.1	15.88
1000	2.4	0.3	3.784	1.674	299	4.927
1500	3.9	0.5	4.323	1.716	445.4	5.226
2000	7.2	0.8	5.232	2.007	585.1	7.734
2500	11	1	5.203	2.213	688.9	5.009
3100	12	1	6.96	2.214	858.8	5.867
3500	10.4	1	6.575	2.107	987	7.704
4000	8.2	1	5.257	2.139	1150	5.631
4500	7.4	1.5	7.231	2.147	1259	6.074
5000	5.3	1	8.74	1.891	1383	6.325
5500	3	0.5	9.553	1.869	1514	9.551
6100	1.3	0.2	8.019	1.971	1637	6.129
6600	1.1	0.2	9.591	1.607	1704	6.432
7200	1.1	0.2	10.62	1.705	1791	7.879
8000	1.2	0.2	9.544	1.914	1925	6.693
8700	1.2	0.2	10.29	1.499	2026	6.68
9300	1	0.2	10.12	1.719	2097	6.052
9600	0.6	0.1	10.46	1.684	2096	6.449

One final note of interest from the data collected is the difference in threshold power for when the forward and backward Stokes beams are manifested. Figure 15 shows that the forward Stokes begins much earlier, but as power increases, the forward Stokes excitation loses efficiency. This may be due to degraded coupling of the pump into the fundamental mode of the fiber. However, the generation of backward Stokes seems to be much less sensitive to this alignment issue. Additionally, higher attenuation at the longer wavelengths created by FWM in the forward Stokes may also account for some of the differences in power between the two propagation directions. However, the true cause of this loss of efficiency is unclear. On the previous page, Table 1 presents the actual figures measured and is included for completeness.

Spectral Data and Results

Spectral measurements were taken first of the RFL seed. At first, it appears that the output is as clean as intended, consisting only of first order Stokes at $1.116\mu\text{m}$ as seen in Figure 16 below. However, Figure 17 below shows a high resolution look at the second order Stokes wavelength of $1.172\mu\text{m}$ and reveals the presence of a very small signal. This is important to keep in mind since any 2nd order Stokes in the amplifier provides a seed to aid the conversion of power in the first order Stokes to the second order Stokes.

The first and second experiments both involved the same length of 5.3km fiber, and differed from each other mainly in the maximum power attainable and how the

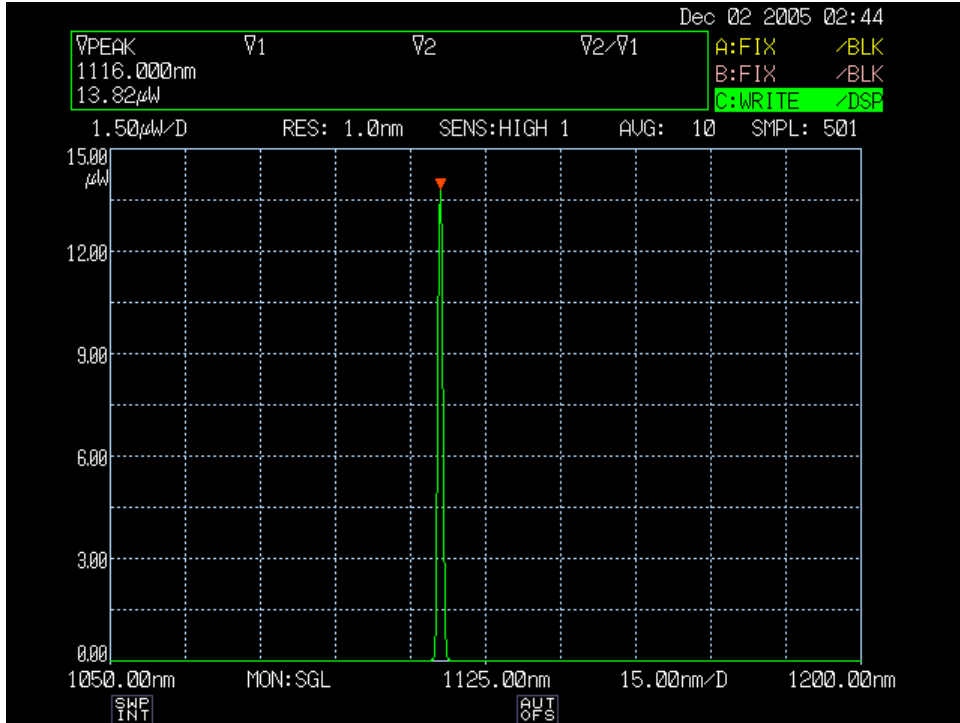


Figure 16. Spectrum of RFL Seed.

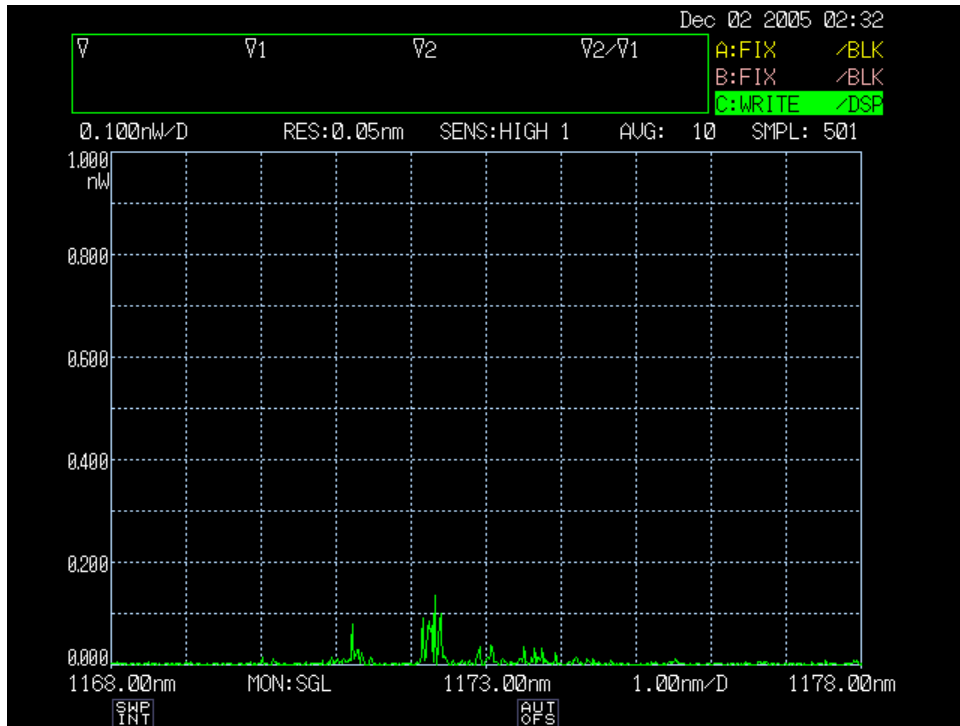


Figure 17. Second Order Stokes Wavelength of RFL Seed.

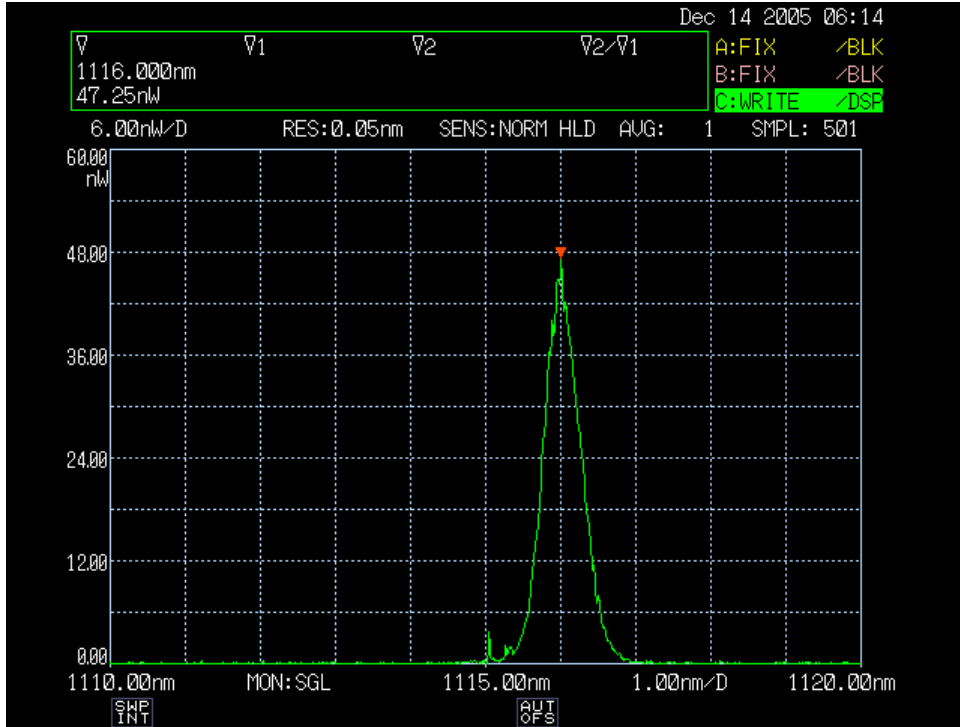


Figure 18. First Order Stokes Spectrum in 5.3km Fiber with $\lambda/2$ Waveplate.

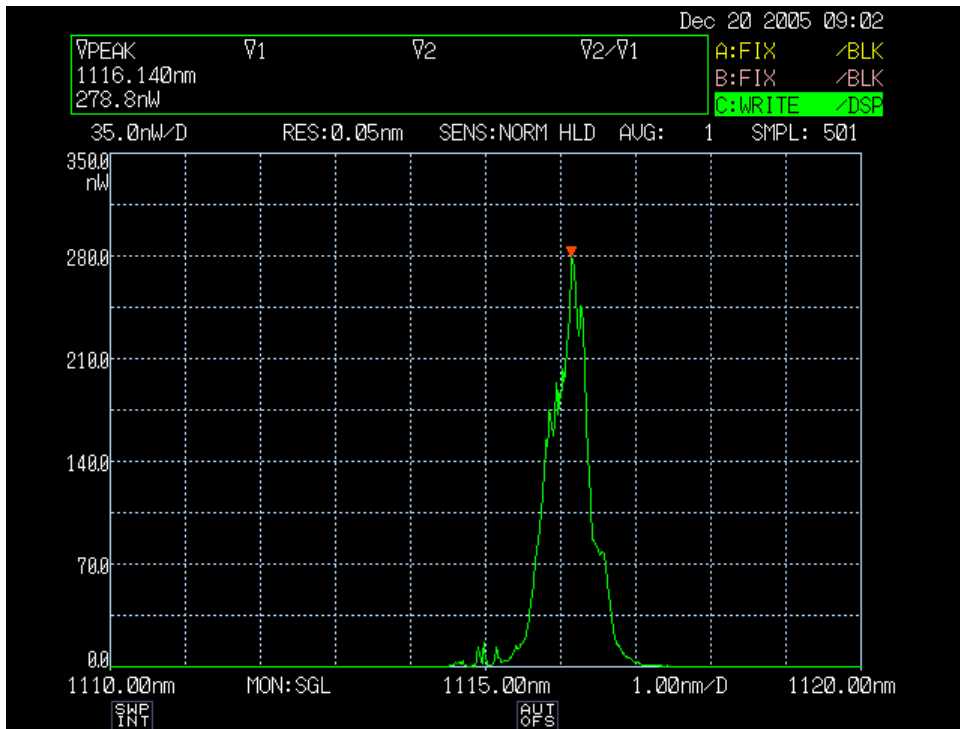


Figure 19. First Order Stokes Spectrum in 5.3km Fiber without $\lambda/2$ Waveplate.

power was controlled. Spectrally, the two do not have important differences in setup. Figure 18 and Figure 19 above show the first order Stokes with 5 W of pumping. The difference in intensity here is primarily due to coupling efficiency into the spectrum analyzer and fluctuations in power of the RFL seed. Figure 20 below shows the first order Stokes from the 2.5km fiber, also with 5 W of pump. It is much higher in intensity since attenuation in the shorter fiber was observed to be much less pronounced. Spectrally though, all three figures show a first order Stokes beam with a full width half maximum (FWHM) of about 0.8nm centered at about 1.1161 μ m. However, the important question is whether FWM is taking place.

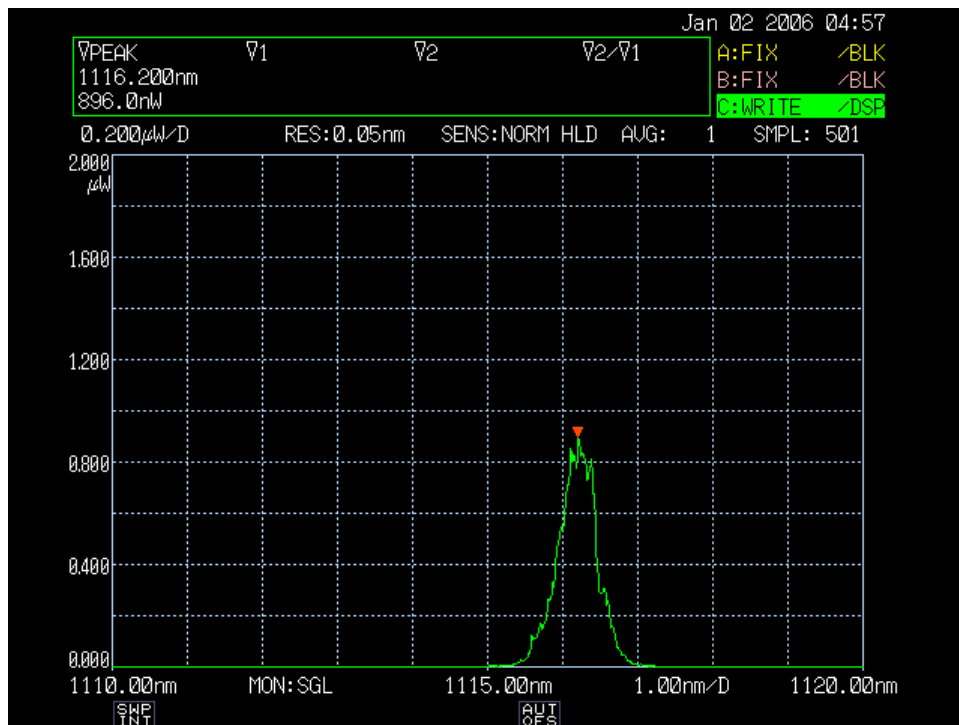


Figure 20. First Order Stokes Spectrum in 2.5km Fiber.

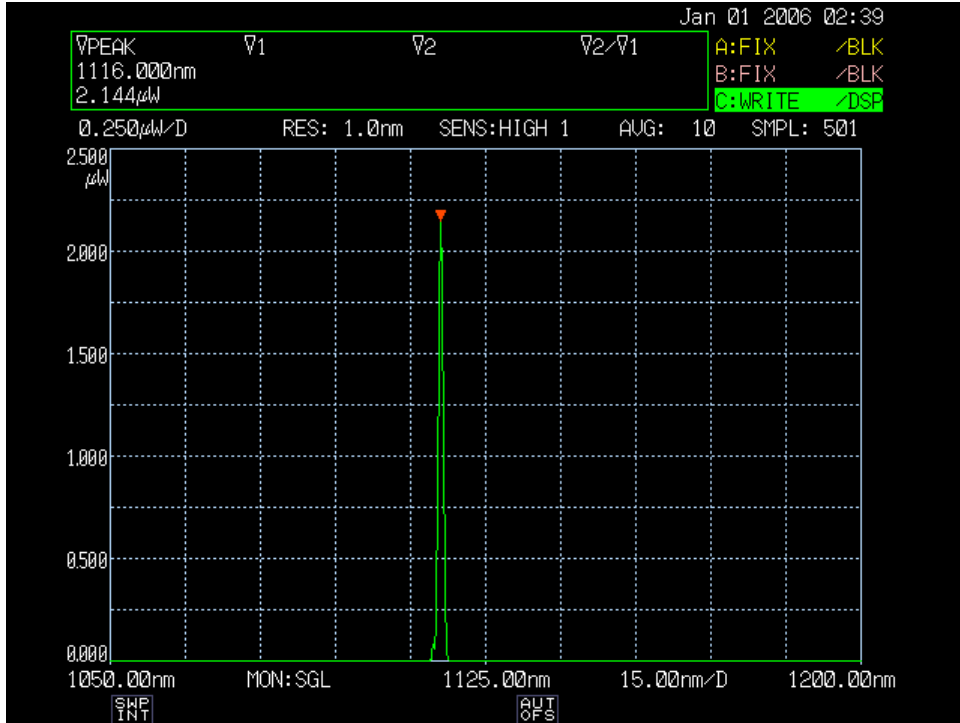


Figure 21. Spectrum of 5.3km Fiber with 10 W of Pump.

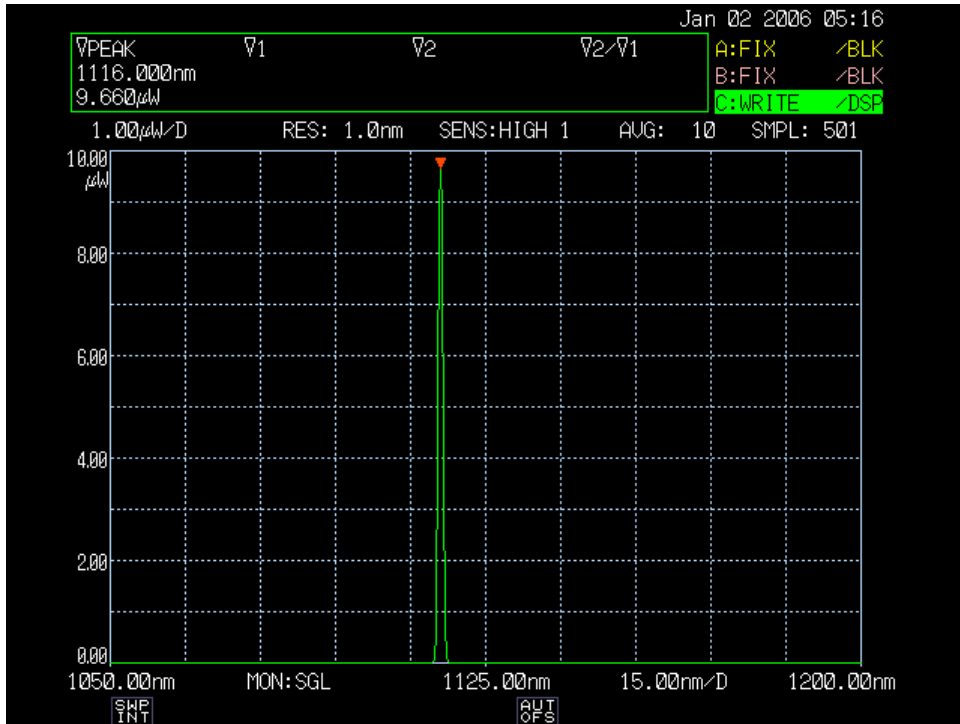


Figure 22. Spectrum of 2.5km Fiber with 10 W of Pump.

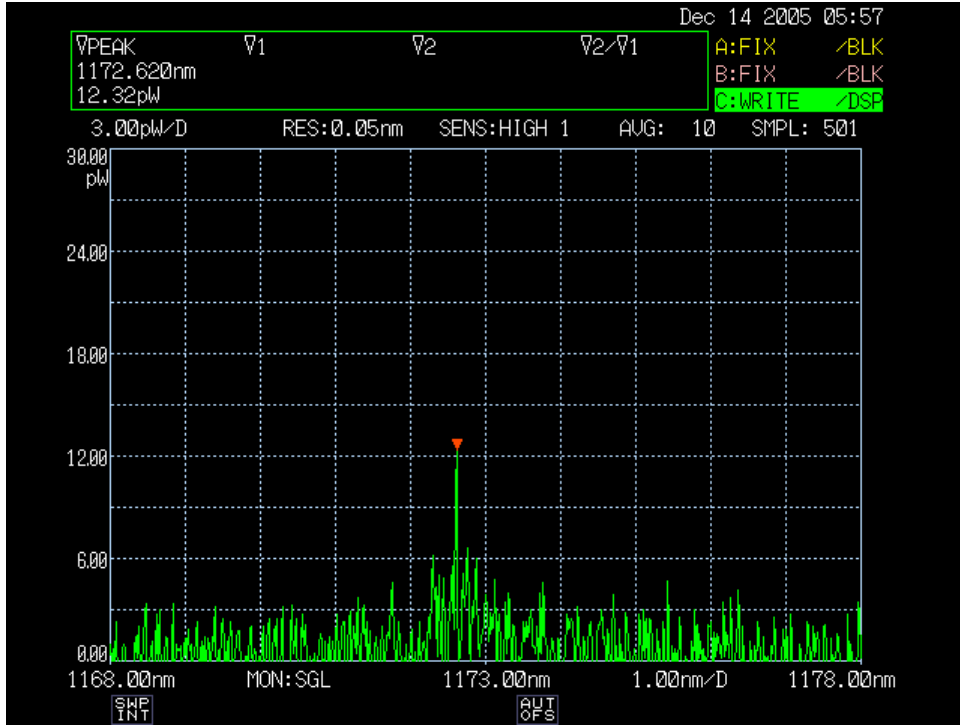


Figure 23. Second Order Stokes Wavelength of 5.3km Fiber with no Pumping.

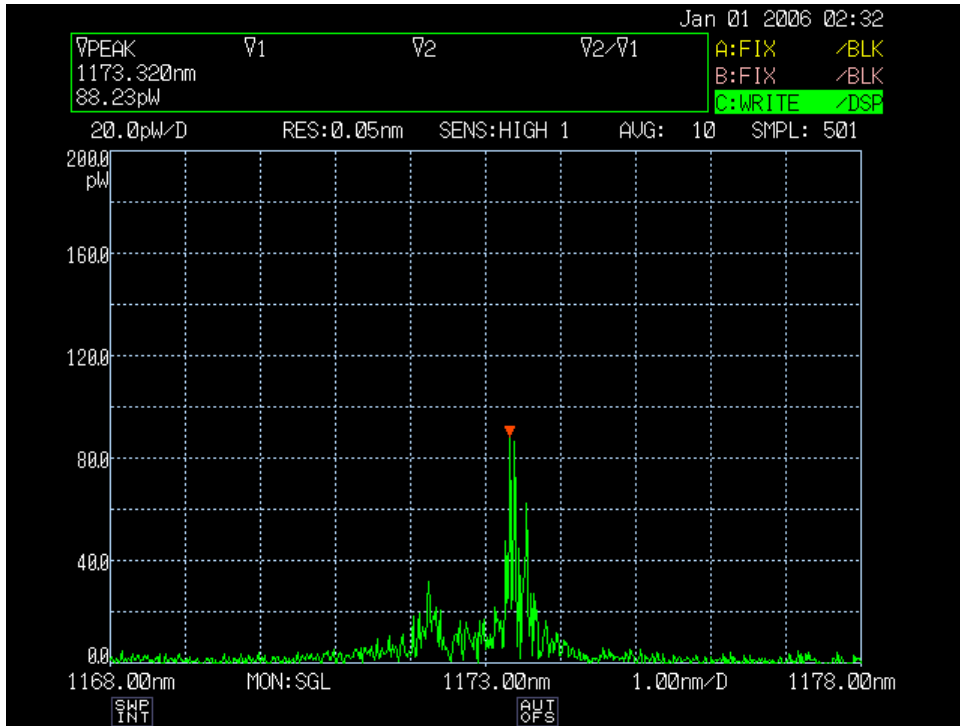


Figure 24. Second Order Stokes Wavelength of 5.3km Fiber with 10 W of Pump.

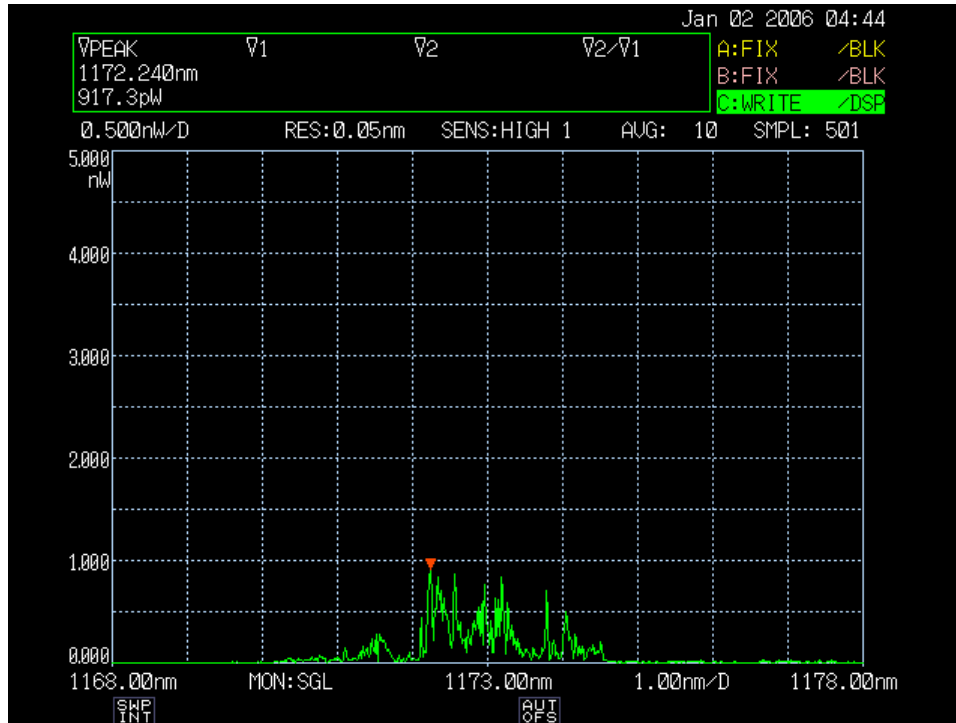


Figure 25. Second Order Stokes Wavelength of 2.5km Fiber with no Pumping.

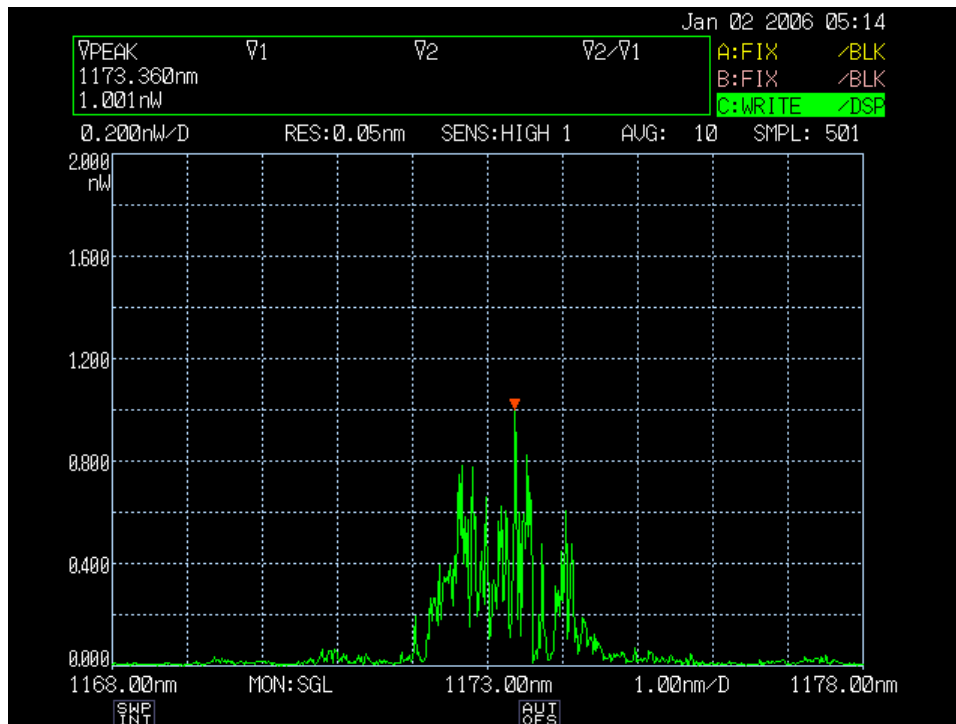


Figure 26. Second Order Stokes Wavelength of 2.5km Fiber with 10 W of Pump.

Figure 11 in the previous section showed FWM with 10 mW of Stokes power in the forward direction with only 3.5 W of pumping and no seed. It is clear from that figure that a substantial amount of the total power exists simultaneously at the first, second, and third order Stokes wavelengths and they are noticeably visible in the spectrum. Even fourth and fifth order Stokes are visible. However, there is no similar sign in the backwards geometry of even the second order Stokes wavelength in Figure 21 and Figure 22 above. A closer look at the second order Stokes wavelength for the 5.3km fiber is shown in Figure 23 and Figure 24. Figure 25 and Figure 26 show the same for the 2.5km. From these figures it is possible to confirm that no significant FWM is taking place even at our maximum level of pumping. In fact, the peak associated with the second order Stokes is very noisy and broad because it is barely above the noise floor and not seeing significant gain. All of the power absorbed from the pump is being used to amplify the first order Stokes.

Beam Profiles and Beam Quality

In order to assess the amount of beam cleanup taking place for each of the experiments, measurements necessary to calculate M^2 were made. Additionally, images of the beam profile were also captured. By comparing the relative size of both the near-field and far-field images, it is possible to get a rough idea of the magnitude of beam cleanup taking place. If the near-field images are the same size, the far-field images of a beam with a markedly better M^2 will be smaller than the far-field image of a beam with a higher M^2 at the same wavelength.

Figure 27 below shows the profile of the CEO pump laser after being coupled through 1m of fiber. The calculated M^2 of the pump was 8.15 ± 0.03 ; however, it was not found to influence the M^2 of the output Stokes beam from the amplifier. The only impact the poor quality of the pump beam had was on the ability to couple power into the fiber efficiently for use in amplification.

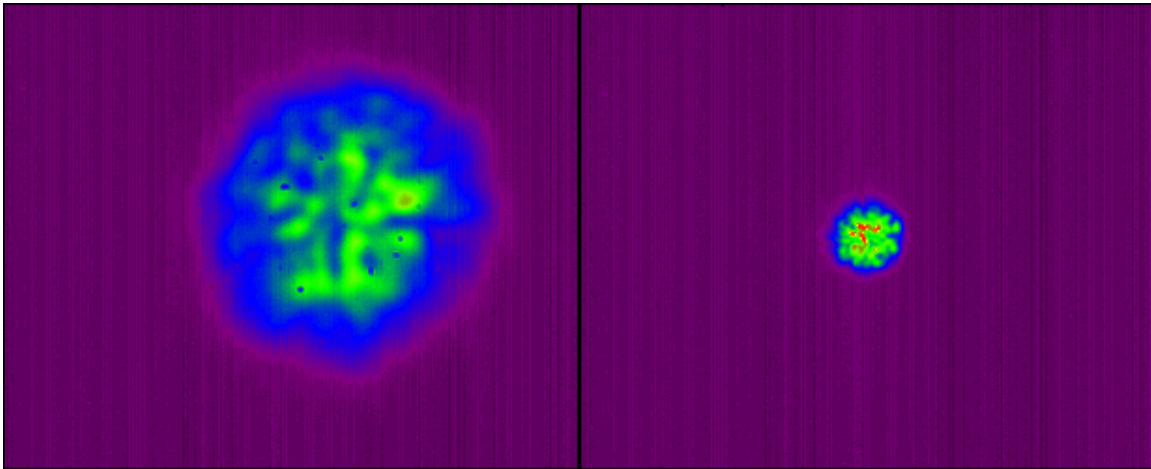


Figure 27. Near-field (left) and Far-field (right) Images of the CEO Pump Laser After 1 Meter of Fiber.

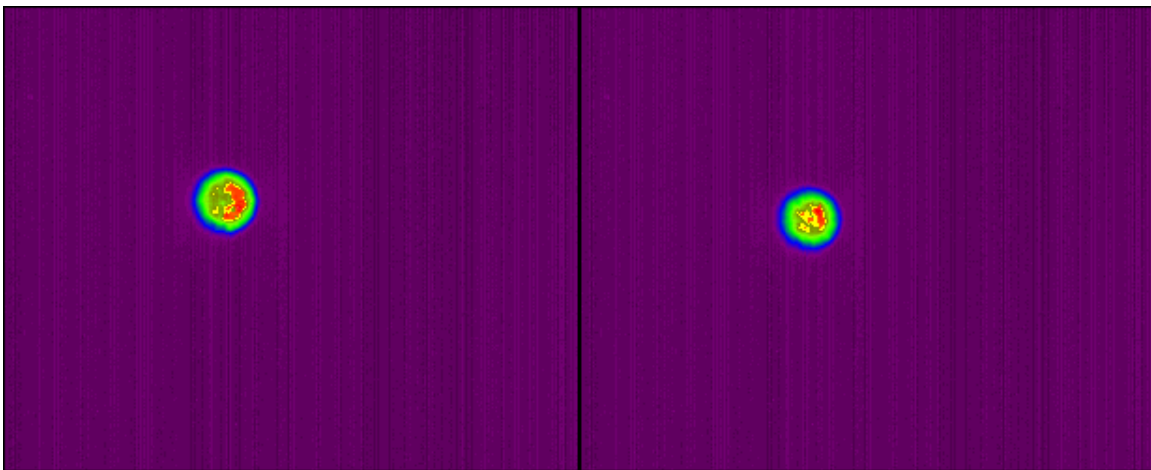


Figure 28. Far-field Images of the Stokes Beam in the 5.3km Fiber with 0 W (left) and 5 W (right) of pump.

In the 5.3km fiber, calculation of the M^2 of the RFL seed after 1m of fiber yielded a value of 7.6 ± 0.1 . After passing through the entire fiber, measurements indicated that the M^2 of the Stokes beam was up to 8.09 ± 0.09 . Once the pump was added, the M^2 of the Stokes output improved, achieving a best value in the 5.3km fiber of 6.7 ± 0.2 for 5 W of pump. Measurement at 10 W of power showed an M^2 of 7.9 ± 0.2 . Figure 28 above shows the far-field images of the unpumped and pumped output from the fiber.

The 2.5km fiber yielded a similar pattern of results to the 5.3km fiber. The RFL seed after 1m of fiber had an M^2 of 4.62 ± 0.08 . This had increased to 4.8 ± 0.1 after passing through the entire fiber, and with 5 W of pump improved to a best value of 3.9 ± 0.5 . 10 W of pump demonstrated an M^2 of 4.3 ± 0.1 . Far-field images for the 2.5km fiber appear below in Figure 29 below.

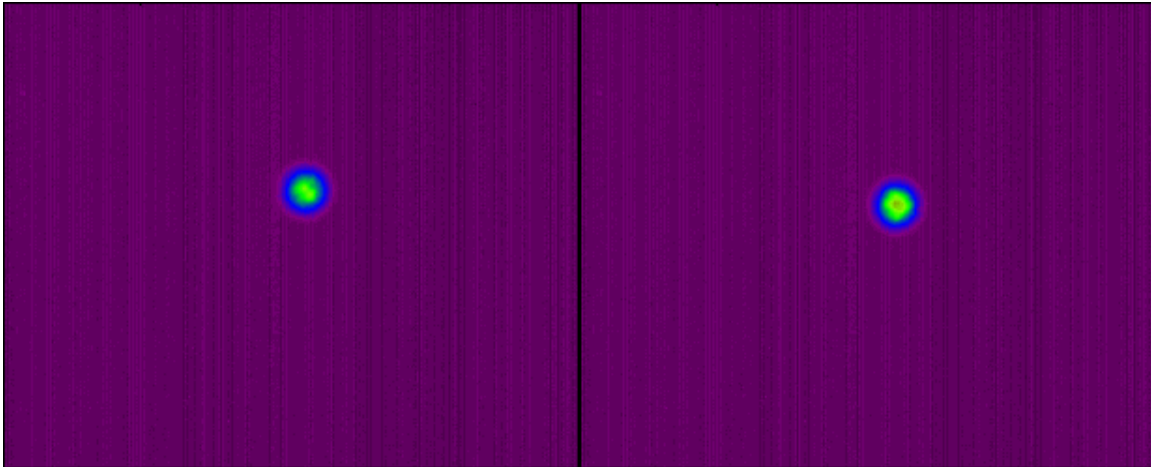


Figure 29. Far-field Images of the Stokes Beam in the 2.5km Fiber with 0 W (left) and 5 W (right) of Pump.

At this point it is important to comment that so few measurements at various powers for calculating M^2 were taken that it would be a mistake to construe any sort of

relation to an optimal pumping level for beam cleanup in the backward geometry. The fact that the beam quality was worse at 10 W for both fibers than at 5 W could be due to a poorer alignment of the pump at this power with the fundamental mode of the fiber. The only clear-cut relationship supported by the data is that pumping slightly improved the beam quality over no pumping, and that the improvement seen was both definite and small. This suggests that the beam quality of the coupled seed may be more important for a backward seeded geometry.

Results of Power Measurements

The power measurements from all three experiments were very consistent. Although the amount of seed was attenuated to a different extent depending on the length of the fiber, as soon as pumping began, an increase in the amount of output Stokes was detected. This indicated gain in the fiber, but for amplification, the output power has to exceed the initial power. In other words, you need enough gain to overcome the attenuation due to the length of fiber.

For each experiment, a measurement of the RFL seed before the fiber amplifier and after 1 meter of fiber was made in order to assess the coupling efficiency. This was used to determine the amount of power actually being coupled into the fiber for use in determining whether amplification was occurring. For example, in the 2.5km fiber, 661 mW was coupled into the fiber out of 843 mW before the fiber. This indicated a coupling efficiency of 78.4% for the alignment. During the time data was being collected on the amount of gain and amplification taking place, 1.04 W of Stokes seed was measured coming from the RFL. Assuming a 78.4% coupling efficiency, this means an initial seed

of 815 mW was actually coupled into the fiber. With no pumping, the fiber had a Stokes output of 516 mW. This indicates an overall attenuation of the Stokes wavelength of 36.7% for this length of fiber (0.8 dB/km). With 10 W of pump, the output Stokes was measured to be 1.248 W. This indicated a gain of 241.8% over the attenuated output of 516 mW and an amplification of 153.1% over the coupled input of 815 mW.

Figure 30 below shows the power readings recorded for the 2.5km fiber, and Figure 31 shows the power for the second set of measurements on the 5.3km fiber. Coupled is the amount of residual pump exiting the front of the fiber with no seed present whereas Depleted shows the amount of residual pump remaining when the seed was present. Stokes is the amount of total Stokes output measured. The graphs do include error bars from the integration times, but they are so small that they are not very visible.

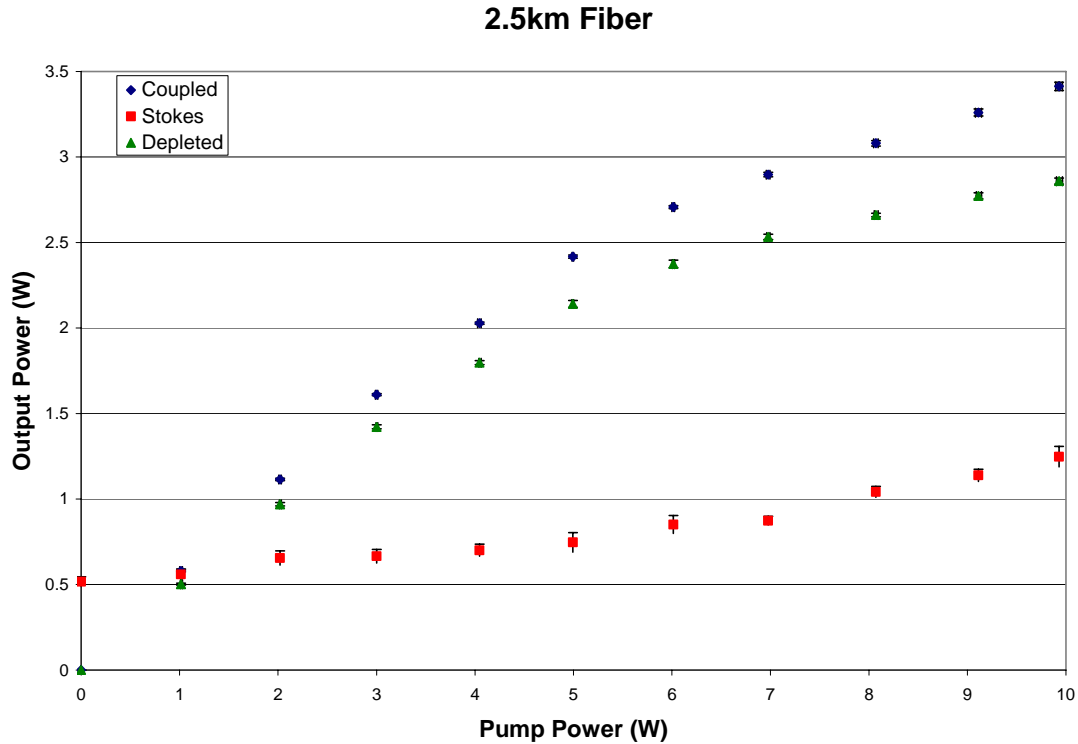


Figure 30. 2.5km Fiber Power Data.

5.3km Fiber, Trial 2

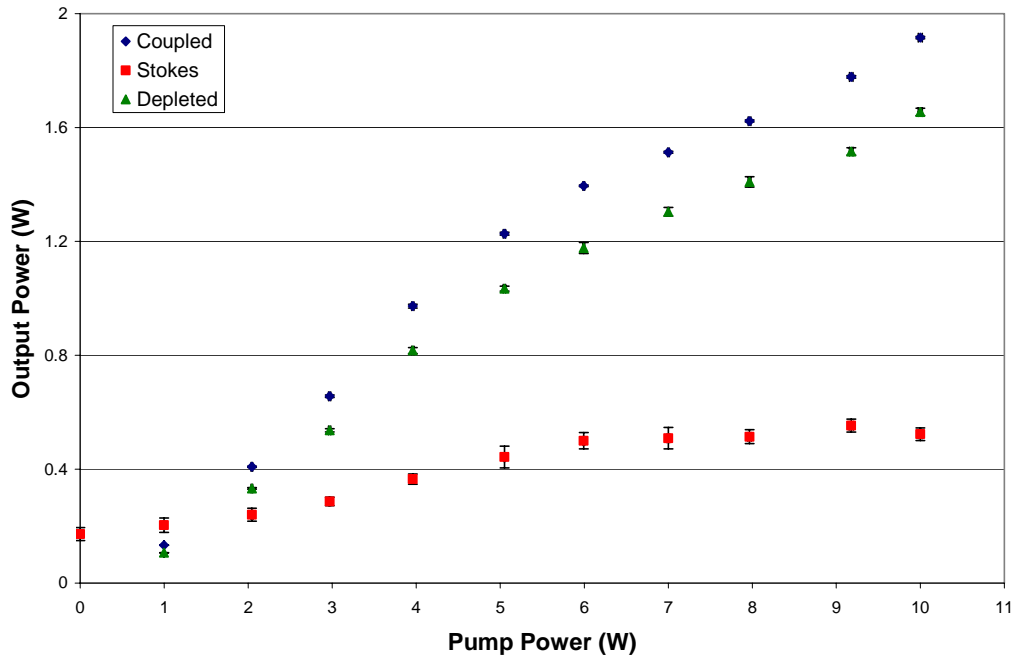


Figure 31. 5.3km Fiber Power Data, 2nd Trial.

Table 2. Standard Deviation of Power Measurements in Watts in 2.5km Fiber.

Pump	Error	Coupled	Error	Stokes	Error	Depleted	Error
	Pump		Coupled		Stokes		Depleted
0	0	0	0	0.5162	0.02858	0	0
1.015	0.01254	0.5797	0.005322	0.5589	0.03278	0.5019	0.005965
2.020	0.01287	1.115	0.006592	0.6551	0.04165	0.9696	0.01009
3.001	0.01276	1.610	0.006253	0.6656	0.03986	1.422	0.01122
4.045	0.01757	2.028	0.006388	0.7008	0.03468	1.797	0.01187
4.993	0.008398	2.417	0.00927	0.7461	0.0567	2.141	0.0198
6.013	0.01321	2.707	0.008649	0.8512	0.05272	2.375	0.02242
6.976	0.01898	2.897	0.01318	0.8735	0.0252	2.533	0.01501
8.071	0.0232	3.080	0.01593	1.042	0.03167	2.661	0.01001
9.112	0.03046	3.260	0.02055	1.139	0.03549	2.772	0.01774
9.931	0.03391	3.413	0.02479	1.248	0.05982	2.859	0.01773

The roll off in Stokes power in Figure 31 is attributed to a combination of decreased overlap of the pump power with the seed and a possible temporal minimum in input seed power. Table 2 on the previous page shows the typical amount of error associated with each of the measurements. As can be seen, the output of the pump beam had approximately one-fifth of the standard deviation for a given amount of power and was therefore much more stable than the Stokes seed. This is attributed to the RFL output, rather than the amplification process. A measurement of the Stokes output of the RFL showed 1.04 W with a standard deviation of 52.36 mW. This error pattern was very consistent for both fibers and for each experiment.

The numbers for the 5.3km fiber indicated a 63.9% coupling efficiency, which translates into 597 mW of seed. The fiber had a Stokes output of 172 mW with no pumping, an overall attenuation of 71.2% for this length of fiber (1.0 dB/km). With 9 W of pump, the output Stokes was measured to be 553 mW. This indicated a gain of 321.3% over the attenuated output of 172 mW, but was just short of amplification at 92.5% over the coupled input of 597 mW. Incidentally, the Stokes output at 10 W was lower than at 5 W at 523 mW, indicating that the higher transverse modes of the pump at 10 W were not as well aligned with the fundamental mode of the fiber.

Summary

This chapter reviewed the data collected from the three experiments. However, the first topic covered was a look at single pass unseeded Raman output. FWM was noted in the forward direction, but not in the backward direction. Next, it was possible to determine from the spectral data from the main three experiments that the backward

pumping geometry also did not suffer from FWM the way a forward pumped configuration suffers from FWM. The beam profiles and beam quality calculations showed that beam cleanup does occur in the backward configuration, but only very weakly and overall beam quality may be strongly influenced by the quality of the original coupled seed beam. The beam quality was not dependent on the quality of the coupled pump, though. Finally, the power data showed that gain occurred in all the fibers. While power was insufficient to show amplification in the longer 5.3km fiber, even without the waveplate setup, it was able to produce amplification in the 2.5km fiber of approximately 150%.

V. Conclusions and Recommendations

Conclusions

The backward pumping geometry does successfully eliminate the problem of FWM. Power remained well confined to the first order Stokes wavelength.

This pumping configuration was also satisfactory for amplifying an initial seed. The 2.5km fiber evidenced an overall amplification of 150% with 10 W of pumping in the fiber. The failure to create actual amplification in the 5.3km fiber was due to the limited available power that could be coupled into the fiber and the amount of attenuation this length of fiber produced that had to be overcome. With more power, the 5.3km fiber would also have experienced amplification of the seed.

However, it appears that there may be a significant drawback to the backward seeded geometry: beam cleanup was very limited. Forward pumping without a seed generally produces a much better beam quality than what was observed with the backward seeded geometry. Although the beam quality data was limited, it appears the backward geometry can improve the beam quality of the seed only by a very limited amount. The best beam quality achieved in the 5.3km fiber was 6.7 ± 0.2 with 5 W of pump, and 3.9 ± 0.5 in the 2.5km fiber also with 5 W of pump. It may be necessary to use a high quality seed if a high quality output beam is desired with the backward geometry.

Future Suggested Work

Through the course of completing this research, several other avenues deserving investigation presented themselves. Due to the limited time constraints and the scope of this project, it will therefore be up to others to complete these explorations. A few of these problems are outlined below.

During my experiments, insufficient data was collected on the output beam quality to allow any trend with the input seed beam's quality to be observed or predicted. It would be desirable to understand and be able to predict the impact on final beam quality that the seed beam has in the backward configuration. Any possible reliance on the amount of beam quality enhancement as a function of the amplification present should also be analyzed.

My experiments dealt exclusively with 50 μm multimode graded index fiber. This type of fiber is also commonly manufactured with core diameters of 62.5 μm and 100 μm diameters. The larger core diameter would facilitate coupling of a higher power, but poorer quality, pump beam. Although the larger diameter decreases the overall power density and consequently the overall gain an amplified seed could attain for a given pump power, it may be possible to more than compensate for this loss with the increased power coupling. These fibers would likely allow even greater levels of amplification, and characterization of this is needed.

Investigation into these areas would further extend our understanding of how to maximize amplification using a backward geometry, while achieving a high beam quality necessary for defense applications. The trade-offs identified would be crucial to our

understanding of how to scale fiber lasers up to the power needed to allow the more maintainable fiber laser to possibly someday replace the chemical lasers of today.

Appendix A

This program uses a nonlinear regression to fit data to the formula for a gaussian laser profile. Data is entered in `denergy` as ordered pairs. `denergy` uses the position `z`, in centimeters, and the diameter of the beam, in micrometers.

```
denergy = {{25, 802.7}, {25.5, 758.8}, {26, 727.9}, {26.5, 693.1}, {27, 672.6}, {27.5, 646.9},
           {28, 626.1}, {28.5, 610.1}, {29, 585.1}, {29.5, 569.5}, {30, 557.6}, {30.5, 551.1}, {31, 539.9},
           {31.5, 537.5}, {32, 543.9}, {32.5, 549.7}, {33, 557}, {33.5, 580.4}, {34, 597.6}, {34.5, 618.8},
           {35, 645.2}, {35.5, 675.2}, {36, 706.8}, {36.5, 737.3}, {37, 768}, {37.5, 797}, {38, 834.9}};
```

This section manipulates the data in `denergy` to convert to common units and to a radius. Also, a best guess is generated for the waist size and position and stored in `waist` and `waistcoord`.

```
Do[Part[denergy, i] = {Part[Part[denergy, i], 1] / 100, Part[Part[denergy, i], 2] / 2000000},
   {i, 1, Length[denergy]}]
zcoord = Take[Flatten[denergy], {1, Length[Flatten[denergy]], 2}];
waistvalue = Take[Flatten[denergy], {2, Length[Flatten[denergy]], 2}];
waist = Min[waistvalue]
waistcoord = Extract[zcoord, First[Position[waistvalue, waist]]]

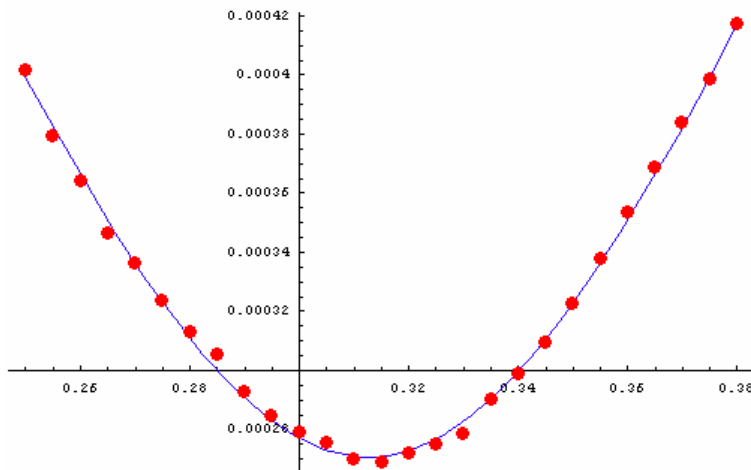
0.00026875

0.315
```

The final part is to enter the appropriate wavelength, do the nonlinear regression, and plot the results along with a calculation of the waist size, position, and value for `M2`.

```
lambda = 1.1165*^-6;
<< Statistics`NonlinearFit`
<< Graphics`Graphics`
nonlinearresult =
  BestFit /. NonlinearRegress[denergy, w0 * Sqrt[1 + (M2 * lambda * (z - z0) / (Pi * w0 ^ 2)) ^ 2],
    z, {{M2, 1}, {w0, waist}, {z0, waistcoord}}, RegressionReport -> {BestFit}];
BestFitParameters /. NonlinearRegress[denergy, w0 * Sqrt[1 + (M2 * lambda * (z - z0) / (Pi * w0 ^ 2)) ^ 2],
  z, {{M2, 1}, {w0, waist}, {z0, waistcoord}}, RegressionReport -> {BestFitParameters}]
DisplayTogether[Plot[nonlinearresult, {z, Min[zcoord], Max[zcoord]}, PlotStyle -> {Hue[.7]}],
  ListPlot[denergy, PlotStyle -> {Hue[0], PointSize[.02]}], ImageSize -> 504]
```

```
{M2 -> 3.58118, w0 -> 0.000270671, z0 -> 0.312479}
```



```
- Graphics -
```

Bibliography

1. Agrawal, Govind P. *Nonlinear Fiber Optics* (Third Edition). San Diego: Academic Press, 2001.
2. Baek, Sung H. and Won B. Roh. "Single-mode Raman Fiber Laser Based on a Multi-mode Fiber," *Optics Letters*, 29(2):153-155 (January 15, 2004).
3. Boeing Image, "Artist's Impression of ABL System in Operations". February 16, 2006 <http://www.boeing.com/defense-space/military/abl/pics-clips/wng2wng.html>.
4. Boyd, Robert W. *Nonlinear Optics* (Second Edition). San Diego: Academic Press, 2003.
5. Chiang, Kin S. "Stimulated Raman Scattering in a Multimode Optical Fiber: Evolution of Modes in Stokes Waves," *Optics Letters*, 17(5):352-354 (March 1, 1992).
6. Islam, Naved R. and Kyohei Sakuda. "Wave-front Reconstruction by Backward-Stimulated Raman Scattering in a Multimode Graded-index Optical Fiber," *Journal of the Optical Society of America*, 14(11):3238-3241 (November 1997).
7. *Multimode Attenuation Measurement Method*. MM21. New York: Corning Inc, [August 2001].
8. Mocofanescu, A., L. Wang, R. Jain, K. D. Shaw, A. Gavrielides, P. Peterson, and M. P. Sharma. "SBS Threshold for Single Mode and Multimode GRIN Fibers in an All Fiber Configuration," *Optics Express*, 13(6):2019-2024 (21 March 2005).
9. Murray, James T., William L. Austin, and Richard C. Powell. "Intracavity Raman Conversion and Raman Beam Cleanup," *Optical Materials*, 11:353-371 (March 1999).
10. "Real Beam Propagation", Excerpt from Online Resource *Optics Guide*. Melles Griot Inc., 2004. February 16, 2006 http://optics.mellesgriot.com/optguide/gb_3_3.htm.
11. Russell, Timothy H., Shawn M. Willis, Matthew B. Crookston, and Won B. Roh. "Stimulated Raman Scattering in Multi-mode Fibers and its Applications to Beam Cleanup and Combining," *Journal of Nonlinear Optical Physics & Materials*, 11(3):303-316 (September 2002).

12. Saleh, Bahaa E. A. and Malvin Carl Teich. *Fundamentals of Photonics*. New York: John Wiley & Sons, 1991.
13. Semrock Image, "Transmission Spectra". February 16, 2006
http://www.semrock.com/Catalog/RamanEdgeFilter_spectra.htm.
14. Terry, Nathan B., Thomas G. Alley, and Won B. Roh. "Brightness Conversion Using a Raman Fiber Laser Based on a Multimode Fiber," *Optical Society of America*, 2005.
15. Verdeyn, Joseph T. *Laser Electronics* (Third Edition). Upper Saddle River NJ: Prentice Hall Inc., 199

REPORT DOCUMENTATION PAGE			<i>Form Approved OMB No. 074-0188</i>		
<p>The public reporting burden for this collection of information is estimated to average 1 hour per response, including the time for reviewing instructions, searching existing data sources, gathering and maintaining the data needed, and completing and reviewing the collection of information. Send comments regarding this burden estimate or any other aspect of the collection of information, including suggestions for reducing this burden to Department of Defense, Washington Headquarters Services, Directorate for Information Operations and Reports (0704-0188), 1215 Jefferson Davis Highway, Suite 1204, Arlington, VA 22202-4302. Respondents should be aware that notwithstanding any other provision of law, no person shall be subject to a penalty for failing to comply with a collection of information if it does not display a currently valid OMB control number.</p> <p>PLEASE DO NOT RETURN YOUR FORM TO THE ABOVE ADDRESS.</p>					
1. REPORT DATE (DD-MM-YYYY) 27-03-2006		2. REPORT TYPE Master's Thesis		3. DATES COVERED (From – To) August 2004 – March 2006	
4. TITLE AND SUBTITLE Backward Amplification and Beam Cleanup of a Raman Fiber Laser Oscillator Using a Multi-Mode Graded Index Fiber Amplifier			5a. CONTRACT NUMBER		
			5b. GRANT NUMBER		
			5c. PROGRAM ELEMENT NUMBER		
6. AUTHOR(S) Morgan, III, Jesse D. S., Captain, USAF			5d. PROJECT NUMBER NAFRL056209093		
			5e. TASK NUMBER		
			5f. WORK UNIT NUMBER		
7. PERFORMING ORGANIZATION NAMES(S) AND ADDRESS(S) Air Force Institute of Technology Graduate School of Engineering and Management (AFIT/EN) 2950 Hobson Way, Building 640 WPAFB OH 45433-7765			8. PERFORMING ORGANIZATION REPORT NUMBER AFIT/GAP/ENP/06-11		
9. SPONSORING/MONITORING AGENCY NAME(S) AND ADDRESS(ES) AFRL/DELO ATTN Rick Berdine 3550 Aberdeen Ave SE Kirtland AFB, NM 87112-5776 505-853-4342			10. SPONSOR/MONITOR'S ACRONYM(S)		
			11. SPONSOR/MONITOR'S REPORT NUMBER(S)		
12. DISTRIBUTION/AVAILABILITY STATEMENT APPROVED FOR PUBLIC RELEASE; DISTRIBUTION UNLIMITED					
13. SUPPLEMENTARY NOTES					
14. ABSTRACT <p>This thesis tested a CW fiber-based Raman amplifier implemented in a backward pumped geometry. To create a seed for the amplifier, a CW Nd:YAG laser operating at 1.064µm was used to pump a 50µm multimode graded index fiber using fiber Bragg gratings to create a Raman Fiber Laser (RFL) Oscillator with a Stokes beam at 1.116µm. The Stokes beam was then used to seed two lengths, 5.3km and 2.5km, of 50µm multimode graded index fiber. The fiber amplifier was pumped by a second CW Nd:YAG laser in the backward geometry.</p> <p>Spectral data taken for both fibers indicated that the backward geometry avoided the problem of Four Wave Mixing (FWM) present in the forward geometry for amplification. Gain and beam cleanup were observed in both lengths of fiber. An M2 of 6.7 ± 0.2 was observed in the 5.3km fiber with 10 W of pumping. With 9 W of pump, a gain of 321.3% was observed, but severe attenuation due to the length of fiber prevented overall amplification of the seed with the available pump power. The 2.5km fiber produced an M2 of 3.9 ± 0.5 with 5 W of pumping. With 10 W of pump, a gain of 241.8% and overall amplification of 153.1% was observed.</p>					
15. SUBJECT TERMS SRS, Raman Scattering, Backward Amplification, Fiber Amplifier, Laser, Beam Cleanup, Multi-mode, Seeded					
16. SECURITY CLASSIFICATION OF:			17. LIMITATION OF ABSTRACT UU	18. NUMBER OF PAGES 66	19a. NAME OF RESPONSIBLE PERSON Thomas Alley, Lt Col, USAF
a. REPORT U	b. ABSTRACT U	c. THIS PAGE U			19b. TELEPHONE NUMBER (Include area code) (937) 255-6565, ext 4649 (thomas.alley@afit.edu)

